Draft version December 17, 2016
Preprint typeset using LaTeX style emulateapj v. 11/26/04

SMASH – SURVEY OF THE MAGELLANIC STELLAR HISTORY

David L. Nidever[1,2,3,4], Knut Olsen[1], Alistair R. Walker[5], A. Katherina Vivas[5], Robert D. Blum[1], Catherine Kaleida[6], Yumi Choi[3], Blair C. Conn[7,8], Robert A. Gruendl[9,10], Eric F. Bell[4], Gurtina Besla[3], Ricardo R. Muñoz[11,12], Carme Gallart[13,14], Nicolas F. Martin[15,16], Edward W. Olszewski[3], Abhijit Saha[1], Antonela Monachesi[17], Matteo Monelli[13,14], Thomas J. L. de Boer[18], L. C. Johnson[19], Dennis Zaritsky[3], Guy S. Stringfellow[20], Roeland P. van der Marel[6], Maria-Rosa L. Cioni[21,22,23], Shoko Jin[24], Steven R. Majewski[25], David Martinez-Delgado[26], Lara Monteagudo[13,14], Noelia E. D. Noël[27], Edouardo Bernard[28], Andrea Kunder[21], You-Hua Chu[29,10], Cameron Bell[21,22],

Draft version December 17, 2016

ABSTRACT

The Large and Small Magellanic Clouds (LMC and SMC) are a unique local laboratory for studying the formation and evolution of galaxies in exquisite detail. As the closest example of an interacting pair of galaxies, they provide special insight into the impact of such interactions on the stellar structure and star formation histories of galaxies. The Survey of the MAgellanic Stellar History (SMASH), a NOAO survey project, is a community DECam survey of the Clouds mapping 480 deg^2 (distributed over $\sim$2400 deg^2 at $\sim$20% filling factor) to $\sim$24th mag griz (and u$\sim$23) – complementing the 5000 deg^2 Dark Energy Survey's partial coverage of the Magellanic periphery – with the goal of identifying broadly distributed, low surface brightness stellar populations associated with the stellar halos and tidal debris of the Magellanic Clouds. SMASH will also derive spatially-resolved star formation histories covering all ages out to large radii of the MCs that will further complement our understanding of their formation. The DECam data have been reduced with a combination of the NOAO Community Pipeline, PHOTRED, an automated PSF photometry pipeline based mainly on the DAOPHOT suite, and custom calibration software. The attained astrometric accuracy is $\sim$20 mas using Gaia DR1 as the astrometric reference catalog, while the photometry precision is $\sim$0.5–0.7% in *griz* and $\sim$1% in u, and the calibration accuracy is $\sim$1.3% in all bands. The SMASH data have been used to discover the Hydra II Milky Way satellite, the SMASH 1 old globular cluster likely associated with the LMC, as well as very extended stellar populations around the LMC out to R$\sim$22°, and more interesting results are in progress. The first public data release contains measurements of $\sim$100 million objects distributed in 61 discrete fields and includes many ancillary data products. A prototype version of the NOAO Data Lab will provide access and exploration tools for the data release, including a custom Data Discovery tool, database access to the SMASH catalog, a Python query interface to the database, an image cutout service, and a Jupyter notebook server with example notebooks for exploratory analysis.

Subject headings: dwarf galaxy: individual: Large Magellanic Cloud, Small Magellanic Cloud — Local Group — Magellanic Clouds — surveys

1. INTRODUCTION

The Large and Small Magellanic Clouds (LMC and SMC), as two of the nearest and most massive satellite galaxies of the Milky Way (MW), offer a unique opportunity to study the processes of galaxy formation and evolution of low-mass galaxies in great detail. They have broad importance for astronomy, with nearly 5000 papers referring to them by keyword, more than the number of citations received by the overview paper of the Sloan Digital Sky Survey (SDSS; York et al. 2000). As the closest example of an interacting pair of galaxies, they provide special insight into the impact of such interactions on the structure and evolution of galaxies. In particular, the Clouds are ideally suited to addressing some critical questions.

What are the consequences of stripping of stars and gas when dwarf galaxies fall into the halos of more massive galaxies, an important mode of mass growth for galaxies since z$\sim$1? What are the properties of the hot and warm gaseous halos of galaxies like the Milky Way, the density of which sets the efficiency of gas stripping and "quenching" of satellites? What are the physical mechanisms and timescales, if any, behind the trigger of star

[1] National Optical Astronomy Observatory, 950 North Cherry Ave, Tucson, AZ 85719 (dnidever@noao.edu)
[2] Large Synoptic Survey Telescope, 950 North Cherry Ave, Tucson, AZ 85719
[3] Steward Observatory, University of Arizona, 933 North Cherry Avenue, Tucson AZ, 85721
[4] Department of Astronomy, University of Michigan, 1085 S. University Ave., Ann Arbor, MI 48109-1107, USA
[5] Cerro Tololo Inter-American Observatory, National Optical Astronomy Observatory, Casilla 603, La Serena, Chile
[6] Space Telescope Science Institute, 3700 San Martin Drive, Baltimore, MD 21218
[7] Research School of Astronomy & Astrophysics, Mount Stromlo Observatory, Cotter Road, Weston Creek, ACT 2611, Australia
[8] Gemini Observatory, Recinto AURA, Colina El Pino s/n, La Serena, Chile.
[9] National Center for Supercomputing Applications, 1205 West Clark St., Urbana, IL 61801, USA
[10] Department of Astronomy, University of Illinois, 1002 West Green St., Urbana, IL 61801, USA
[11] Departamento de Astronomía, Universidad de Chile, Camino del Observatorio 1515, Las Condes, Santiago, Chile
[12] Visiting astronomer, Cerro Tololo Inter-American Observatory, National Optical Astronomy Observatory, which is operated by the Association of Universities for Research in Astronomy (AURA) under a cooperative agreement with the National Science Foundation.

formation by galaxy interactions?

A decade ago, the interaction history of the Magellanic Clouds (MCs) was thought to be well understood, with only minor details remaining to be explained. The gaseous Magellanic Stream, Leading Arm and Bridge were well reproduced by a model invoking tidal stripping through repeated close passages to the MW by the MCs on their bound orbit (e.g., Gardiner & Noguchi 1996). However, in the last decade, several important discoveries have been made about the MCs that raise fresh questions about their structure and past evolution. Perhaps most surprising is the discovery, based on recent HST proper motions of the MCs (Kallivayalil et al. 2006; Kallivayalil et al. 2006; Kallivayalil et al. 2013), that the MCs are likely approaching the MW environment for the first time (Besla et al. 2007). This discovery has forced a reinterpretation of many features of the Magellanic System, leading recent simulations (Besla et al. 2010, 2012; Diaz & Bekki 2012) to conclude that LMC-SMC interactions alone are responsible for the formation of the Magellanic Bridge, Stream, and Leading Arm, HI features now known to extend for at least 200° across the sky (Nidever et al. 2010).

The consequences of this new picture for the stellar component of the MCs are only beginning to be explored. Nevertheless, we now know that MC stellar populations can be found over vast areas of sky (∼22°away from the LMC, Muñoz et al. 2006); that the LMC has stripped a large number of stars from the SMC (∼5% of the LMC's mass, Olsen et al. 2011); and that strong population gradients exist to large radii (Gallart et al. 2008; Cioni 2009). In addition, the advent of the ∼5000 deg^2 Dark Energy Survey (The Dark Energy Survey Collaboration 2005) has given rise to the discovery of many new satellite galaxies (Bechtol et al. 2015; Koposov et al. 2015; Drlica-Wagner et al. 2015) some of which may be associated with the Magellanic Clouds (Deason et al. 2015; Jethwa et al. 2016; Walker et al. 2016). Furthermore, Mackey et al. (2016) detected a "arc-like" structure in the periphery of the LMC (at ∼15° from the center) which is likely a tidally disturbed portion of the LMC disk. These results point to a much richer and more complex structure and history than was imagined just a few years ago.

Most previous survey were based on pencil-beam searches of only ∼1% of the relevant area. With the advent of large imagers such as the Dark Energy Camera (DECam) on NOAO's 4-meter Blanco telescope, the door was opened to pursue a more systematic study of the Magellanic environs.

Our Survey of the MAgellanic Stellar History (SMASH) aims to measure the extended stellar populations of the Clouds and allow us to develop general ideas regarding galaxy evolution in quantitative detail. SMASH is NOAO survey project using DECam to map 480 deg^2 of the Magellanic periphery (distributed over ∼2400 deg^2 at ∼20% filling factor) with deep *ugriz* images. Using old main sequence stars as tracers, our survey will reveal the relics of the formation and past interactions of the Clouds down to surface brightnesses equivalent to Σ_g=35 mags arcsec^{-2}. The main project goals are:

- Search for the stellar component of the Magellanic Stream and Leading Arm. The detection of stellar debris in these structures would make them the only tidal streams with known gaseous and stellar components in the Local Group. This would not only be invaluable for understanding the history and observable consequences of the Magellanic interaction, but would give us a dynamical tracer of the MW's dark halo and a way to probe the MW's hot halo gas via ram pressure effects.

- Detect and map the smooth components of the Clouds, including their extended disks and potential stellar halos. The size of the LMC's stellar disk is a direct probe of the tidal radius of the LMC, with which we can explore the dark matter halos of the LMC and MW.

- Detect and map potential streams and substructure in the Magellanic periphery not associated with HI features. These would probe stages in the formation and interaction of the Clouds at times earlier than the HI dissipation timescale.

- Derive spatially resolved, precise star formation histories covering all ages of the MCs and to large radii, thus providing detailed information on their complete evolution.

- Enable many community-led projects, including studies involving the LMC/SMC main bodies, Galactic structure, discovery of variable objects, and background galaxy populations.

The layout of this paper is as follows. Section 2 and 3 detail the survey and observing strategy. An overview of the data reduction is given in Section 4 while the calibration is discussed in Section 5.2. The details of the

[13] Instituto de Astrofísica de Canarias, La Laguna, Tenerife, Spain
[14] Departamento de Astrofísica, Universidad de La Laguna, Tenerife, Spain
[15] Observatoire astronomique de Strasbourg, Université de Strasbourg, CNRS, UMR 7550, 11 rue de l'Université, F-67000 Strasbourg, France
[16] Max-Planck-Institut für Astronomie, Königstuhl 17, D-69117 Heidelberg, Germany
[17] Max-Planck-Institut für Astrophysik, Karl-Schwarzschild-Str. 1, 85748 Garching, Germany
[18] Institute of Astronomy, University of Cambridge, Madingley Road, Cambridge CB3 0HA, UK
[19] Center for Astrophysics and Space Sciences, UC San Diego, 9500 Gilman Drive, La Jolla, CA, 92093-0424, USA
[20] Center for Astrophysics and Space Astronomy, University of Colorado, 389 UCB, Boulder, CO, 80309-0389, USA
[21] Universität Potsdam, Institut für Physik und Astronomie, Karl-Liebknecht-Str. 24/25, 14476 Potsdam, Germany
[22] Leibniz-Institut für Astrophysics Potsdam (AIP), An der Sternwarte 16, 14482 Potsdam Germany
[23] University of Hertfordshire, Physics Astronomy and Mathematics, Hatfield AL10 9AB, United Kingdom
[24] Kapteyn Astronomical Institute, University of Groningen, P.O. Box 800, 9700 AV Groningen, The Netherlands
[25] Department of Astronomy, University of Virginia, Charlottesville, VA 22904, USA
[26] Astronomisches Rechen-Institut, Zentrum für Astronomie der Universität Heidelberg, Mönchhofstr. 12-14, 69120 Heidelberg, Germany
[27] Department of Physics, University of Surrey, Guildford, GU2 7XH, UK
[28] Lagrange, Observatoire de la Côte d'Azur, Nice, France
[29] Institute of Astronomy and Astrophysics, Academia Sinica, No.1, Sec. 4, Roosevelt Rd, Taipei 10617, Taiwan, R.O.C.

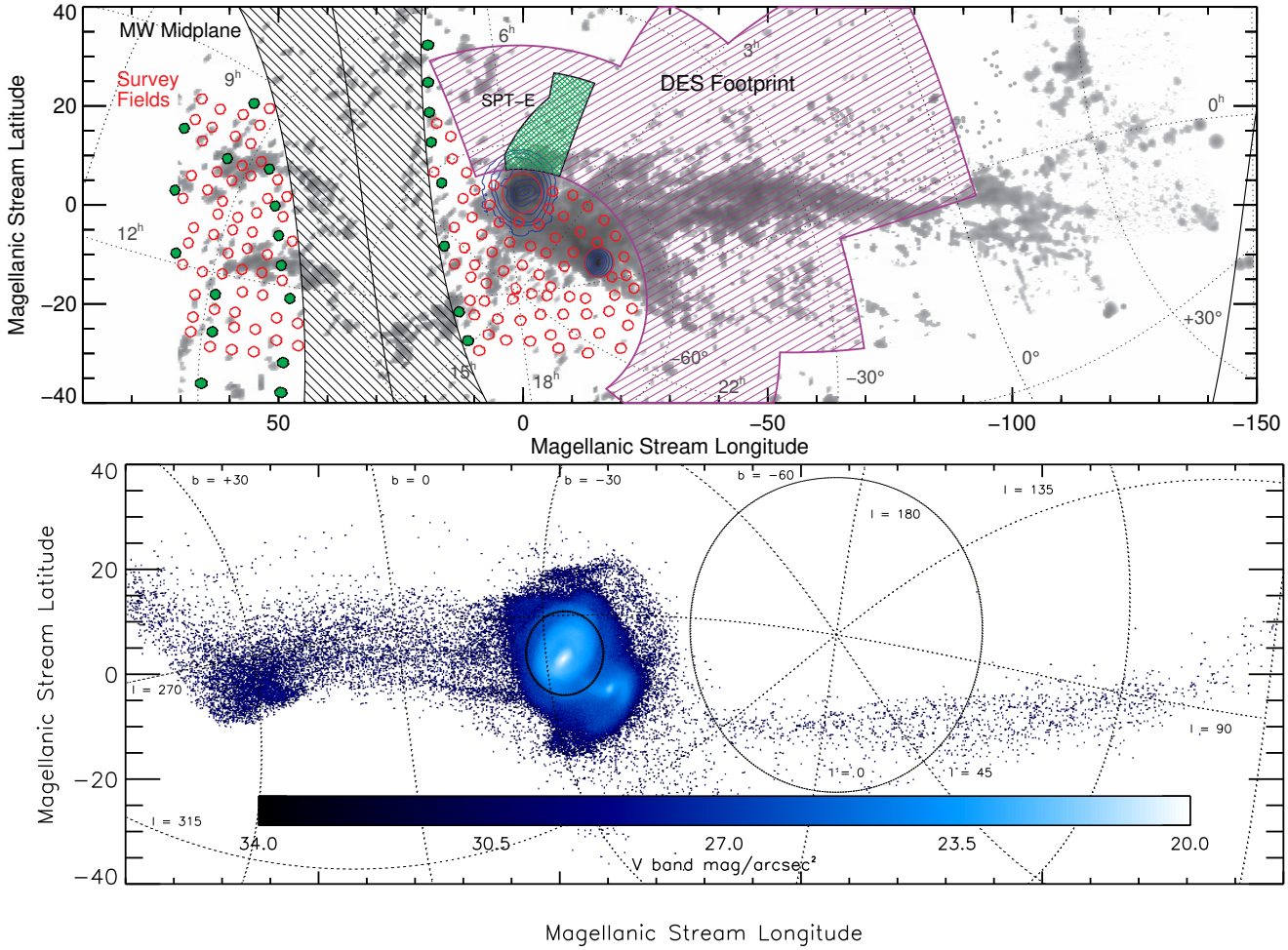

FIG. 1.— (Top) The observed H I column density of the entire 200° Magellanic Stream system is shown in grayscale (Nidever et al. 2010), while the blue contours represent the 2MASS RGB starcounts. The DES footprint is represented by the purple shaded region which also contains the DES full-depth 175 deg^2 SV commissioning SPT-E field (green). Our 23 DECam March 2013 fields for the Leading Arm proposal (2013A-0411) are shown as green hexagons. Our target fields for this proposal are indicated by open red hexagons and large circles (for the main bodies of the MCs). (Bottom) The predicted V-band surface brightness (mag/arcsec^2) of the stellar component of the Magellanic system from Besla et al. (2013). The simulation predicts stellar structures out to large radii from the main bodies of the Magellanic Clouds (varying on small scales), and a higher stellar density in the Leading Arm (*not* covered by the Dark Energy Survey, DES) than in the trailing Stream. TOP FIGURE NEEDS TO BE UPDATED.

first SMASH data release and data access are described in Section 6 and, finally, some of the first SMASH science results are discussed in Section 7.

2. SURVEY STRATEGY

Figure 1 shows the region of the sky that is relevant to the Magellanic Clouds and the Magellanic Stream, with the HI distribution in the top panel and the predicted stellar distribution of the (Besla et al. 2013) model in the bottom panel. The DES footprint already covers one half of the LMC/SMC periphery as well as most of the trailing Magellanic Stream. We decided to design the SMASH footprint to cover the rest of the Magellanic periphery and the Leading Arm, but avoiding the Milky Way mid-plane that could "contaminate" the data. A fully-filled survey would have been preferred, but to reach the sensitivity required to detect the predicted low surface brightness features would have required hundreds of nights and would be beyond the possibility of a NOAO survey proposal. We, therefore, decided to pursue a deep but partially-filled survey strategy as is shown in the top of Figure 1 (hexagons). The SMASH fields map an area of ∼480 deg^2 but are distributed over (and probe the stellar populations of) ∼2400 deg^2 with a filling factor of ∼20%.

We chose fields using an all-sky tiling scheme in which we laid down a uniform hex pattern of field centers with 1.7° separation between field centers, with coordinates based on an Interrupted Mollweide projection. This spherical projection has low distortion, such that a uniform sampling in its coordinate system produces tiling with few areas of excessive overlap between fields. We then transformed the coordinates of the hex-based tiling to spherical coordinates, and rotated the coordinate system to place the seams and poles (southern pole of $[\alpha,\delta]=[10°,-30°]$) in areas outside of our survey area. Our resulting tiling of the sky was nearly uniform over our survey area with ∼15% overlap between fields to allow for good cross-calibration with neighboring fields.

From this list of tiles we selected fields by hand to uniformly cover the region of interest with a ∼20% filling

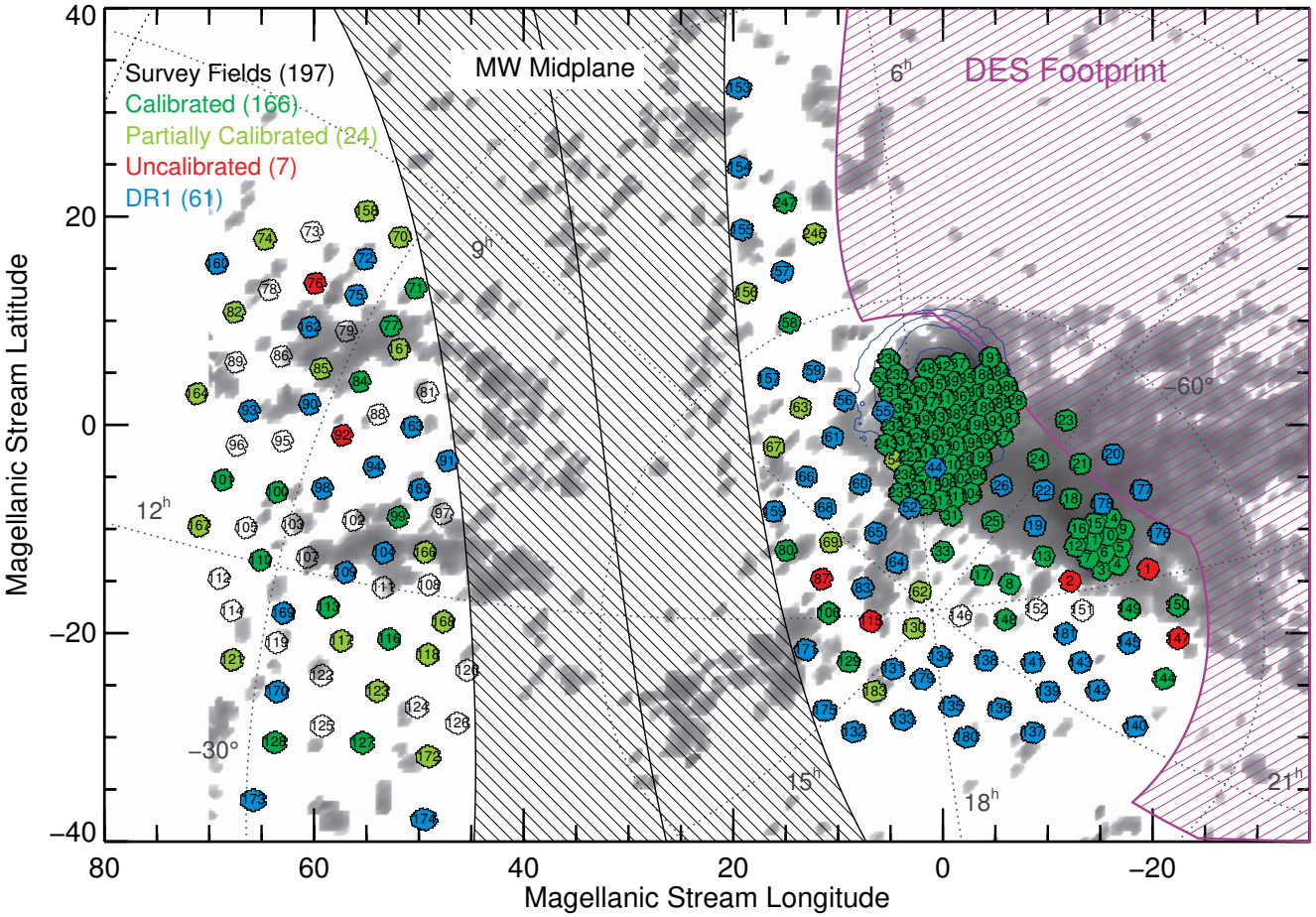

FIG. 2.— The SMASH survey. The observed HI column density of the Magellanic Stream system is shown in grayscale (Nidever et al. 2010). SMASH fields already observed are shown as filled hexagons while unobserved SMASH fields are indicated by open black hexagons. Green (and dark blue) fields are fully calibrated (166 fields), light green are partially calibrated (24 fields), and red are uncalibrated (7 fields). The 61 DR1 fields are shown in dark blue (all fully calibrated). The DES footprint is represented by the purple shaded region. Note that even though the SMASH fields were designed to be complementary to the DES survey, the DES footprint changed over the last couple of years producing some overlap and gaps between the two surveys.

factor as well as fully sample the inner regions of the LMC and SMC which produced 154 fields. The full coverage tiling scheme and overlap was used so that we could more easily fully-fill regions with interesting stellar populations later on, which is what we did for the outer LMC disk. Note that the final survey tiling scheme was created after the 2013, March 17-20 pre-survey run. Therefore, the 23 Leading Arm fields (Fields 153 – 175) that were observed on that run on not entirely on the final tiling scheme but not very far off. The final list of SMASH fields with coordinates in various systems is available in `data/smash_fields_final.txt` on the SMASHRED[30] repository.

3. OBSERVING STRATEGY AND OBSERVATIONS

The idea for SMASH was conceived during the NOAO "Seeing the Big Picture: DECam Community Workshop" in Tucson, AZ on August 18–19, 2011. We decided to submit a proposal for a Magellanic Clouds pilot project using Science Verification (SV) and Shared Risk (SR) time during the 2012B season. The goal of the successful project (SV:2012B-3005 and SR:2012-0416) was to ascertain the necessary filters and depth to attain the needed sensitivity to Magellanic stellar populations. Data were obtained in five fields at various distances from the Magellanic Clouds and included exposures in all five *ugriz* bands and to a depth ∼1 mag deeper than we thought was necessary for our science goals. These data helped us evaluate various observing and survey strategies. Ultimately, it was decided that all five band would give us the best sensitivity to Magellanic stellar populations, although the data are not quite as deep in u and z as the other bands.

After the pilot project, there was no call for survey proposals, so we proceeded to submit a regular NOAO proposal to look for stellar populations in the area of the Leading Arm (2013A-0411). To maximize the coverage we did not take u-band exposures for this observing run, however, the u-band exposures were obtained on later observing runs.

There was a call for survey proposals during the next semester, and we submitted a successful proposal for the SMASH survey of the Magellanic Cloud stellar populations (2013B-0440). We were originally awarded 30 DECam nights (with a 7/3 A/B semester split) and 14 0.9m nights for calibration purposes over three years. The

[30] https://github.com/dnidever/SMASHRED

standard SMASH observing sequence for a science field is three 60 second exposures (with large half chip offsets) in each band and three deep exposures with exposure times of 333/267/267/333/333 seconds in $u/g/r/i/z$ (with small $\sim 2''$ dithers). Each field takes about 110 min. to observe including readout time and slewing. Each night exposures of four to five standard star fields (focusing on the SDSS equatorial region where data for all chips could be obtained simultaneously) were obtained with exposure times of 1 sec. in all *ugriz* bands and 10 sec. in *griz* and 60 sec. in u, but this was later reduced to 15 sec. in *griz* and 60 sec. in u half-way through the survey.

Due to bad weather, poor seeing (we have seeing constraints for the central LMC/SMC main-body fields because of crowding), and the short B semester nights, the survey fell behind in the main-body regions. Therefore, after the first year we requested our 10 nights per year be split evenly between the A and B semester (instead of 7/3 as before), and after the second year, an additional three nights per semester in 2015B and 2016A. After our last year, we requested a three night extension in 2016B to fill a "hole" in our coverage of the SMC periphery (near the south celestial pole) of 11 fields. Additional DECam nights were obtained through the Chilean TAC (PI: Muñoz; 2014 Jan. 21–28). Finally, after the discovery of the Hydra II Milky Way satellite in the SMASH data (Martin et al. 2015), we submitted a Director's Discretionary Time proposal to obtain time-series data on Hydra II to study variable stars (2015 March 30+31).

On our very successful 2016 Feb 13–18 run, we finished all of the fields around the Magellanic Clouds that were observable and, therefore, we decided to observe some "extra" shallow fields around the LMC that would help reveal structures in the LMC disk (similar to those seen by Mackey et al. 2016 and Besla et al. 2016) and allow us to create a more homogeneously calibrated dataset around the LMC using an ubercal technique. The last SMASH observing run in the Leading Arm region (2016 May 8–12) was completely lost due to bad weather, and, therefore, the Leading Arm fields were not completed.

Table 1 shows all SMASH observing including time and data from non-NOAO survey sources. More information about which nights were photometric are in the `smash_observing_conditions.txt` file (see section 5.1 below).

3.1. *0.9-m Observations*

The CTIO 0.9-m telescope and Tek2K CCD camera were used to collect observations of SDSS standards and SMASH fields in order to provide an independent calibration of a portion of the DECam data, particularly for fields observed under non-photometric conditions with the 4-m telescope. The bulk of these observations were taken using CTIO's SDSS *ugriz* filter set, while for three nights we used the borrowed DES PreCam *griz* filters for the sake of comparison.

The typical nightly observing plan in photometric weather was to observe several standard star fields from Smith et al. (2002) and from SDSS Stripe 82 and Stripe 10 (DR12; Alam et al. 2015) at the beginning and end of each night and every $\sim$2 hours in between, and observe SMASH fields during the rest of the time. The Tek2K camera has a $13.5' \times 13.5'$ field of view, and so covered only the central portion of the SMASH fields. We did not offset the 0.9-m to cover the full DECam field of view, and so provided calibration information only for the central DECam chips. Typical exposure times for the standard fields were 300 s (u), 20 s (g), 5s (r), 10s (i), and 15 s (z), while for the smash fields we took sets of five undithered exposures with individual exposure times of 600 s (u), 60 s (g), 60s (r), 120s (i), and 360 s (z). During non-photometric 0.9-m nights, we only took images of SMASH fields, and used short exposures of these fields taken on photometric nights to bootstrap the calibration of the non-photometric exposures. Table 1 also summarizes the 0.9-m observing runs.

Calibration data taken at the telescope consisted of daily dome flats in *griz*, twilight sky flats in *ugriz*, exposures for the creation of a shutter shading map, and exposures for the creation of a bad pixel mask. The shutter shading calibration data consisted of r-band dome flats observed while repeatedly opening the shutter for one second and closing it during the exposure, intermingled with normal dome flats taken with the same total exposure time as the shutter frames. The bad pixel mask data consisted of 100 0.1-second r-band dome flat exposures and a set of 6 r-band dome flats taken with levels equaling 75% of saturation.

4. DATA REDUCTION

The SMASH data reduction of the DECam data makes use of three separate software packages: (1) the Community Pipeline for instrument signature removal, (2) PHOTRED[31] for PSF photometry, and (3) SMASHRED, custom software written for PHOTRED pre- and post-processing of the SMASH data.

4.1. *Community Pipeline Reductions*

The NOAO DECam Community Pipeline (CP; Valdes et al. 2014)[32] was jointly developed by the Dark Energy Survey Data Management (DESDM) team and NOAO (mainly by F. Valdes) to produce reduced images for the community. The CP performs the following operations on the data:

- Bias correction.
- Crosstalk correction.
- Saturation masking.
- Bad pixel masking.
- Linearity correction at both low and high count levels.
- Flat field calibration.
- Fringe pattern subtraction, for z and Y bands.
- Bleed trail and edge bleed masking and interpolation.
- Astrometric calibration of the image WCS with 2MASS as the astrometric reference catalog.

[31] https://github.com/dnidever/PHOTRED
[32] http://www.noao.edu/noao/staff/fvaldes/CPDocPrelim/PL201_3.html

TABLE 1
SMASH DECam and 0.9m Observing Runs

Date (nights)	Telescope	Source	Comments
Pre-Survey			
Dec 11+12, 2012 (2)	4m	Shared Risk	5 pilot fields
Mar 17–20, 2013 (4)	4m	2013A-0411	23 fields (griz)
Aug 8+9, 2013 (2 part)	4m	Time from other project	clear, 3 fields
Survey Year 1			
Sep 7–10, 2013 (4)	0.9m	NOAO survey	bad weather, no data
Sep 11–13, 2013 (3)	0.9m	Bought from SMARTS	bad weather, no data
Oct 21+22, 2013 (2 part)	0.9m	Makeup for Sep 11–13	bad weather, no data
Jan 5–7, 2014 (3)	4m	NOAO survey	0.5 night lost, 10 fields
Jan 12+13, 2014 (2)	0.9m	Makeup for Oct 21+22	2 nights photometric, 4 fields calibrated
Jan 19+20, 2014 (2 half)	4m	DD time	clear, riz for 6 fields
Jan 21–28, 2014 (8 half)	4m	Chilean time	1 half nts lost, 4 fields, 9 partials
Jan 29+30, 2014 (2 half)	4m	DD time	clear, ug for 8 pre-survey fields
Feb 13, 2014 (1 part)	4m	Engineering	clear, riz for 6 fields
Feb 14–23, 2014 (10)	0.9m	NOAO survey	9 nts photom., 30 fields calibrated
May 27–June 2, 2014 (7)	4m	NOAO survey	lost 1 nt, 21 fields observed, ug for 13 pre-survey fields, 3 extra fields
Survey Year 2			
Sep 25–Oct 1, 2014 (7)	0.9m	NOAO survey	1 nt photometric, 11 fields calibrated
Oct 11–12, 2014 (2)	4m	Engineering	some globular cluster calibration data
Nov 21–23, 2014 (3)	4m	NOAO survey	12 LMC/SMC main-body fields
Dec 17–18, 2014 (2)	4m	NOAO survey	8 LMC/SMC main-body fields
Mar 13–18, 2015 (5)	4m	NOAO survey	mostly clear, 21 finished, 4 partials
Mar 30–31, 2015 (2)	4m	DD time	deep & high-cadence data of Hydra II
Apr 26–Mar 2, 2015 (7)	0.9m	NOAO survey	4.5 nts photom., 48 fields calibrated
Survey Year 3			
Oct 25+27, 2015 (2)	4m	DD time	bad weather, no data
Nov 9, 2015 (1)	4m	NOAO survey	clear, 4 fields
Nov 23, 2015 (1)	4m	DD time	bad weather, long riz for 2 fields
Nov 27–29, 2015 (3)	0.9m	Chilean time	9 fields calibrated
Dec 5+6, 2015 (2)	4m	NOAO survey	8 fields, 7 are LMC/SMC main-body
Jan 1–6, 2016 (6)	4m	NOAO survey	4 nts lost, 3 finished, 2 partials
Feb 13–18, 2016 (6)	4m	NOAO survey	40 shallow LMC fields, 18 long fields
May 8–12, 2016 (5)	4m	NOAO survey	bad weather, no data
Survey Year 4 – Extension			
Oct 29–31, 2016 (3)	4m	NOAO survey	0.5 night lost, 8 fields

- Single exposure cosmic ray masking, by finding pixels that are significantly brighter than their neighbors.
- Photometric calibration using USNO-B1.
- Sky pattern removal. The "pupil ghost" and spatially varying background are subtracted.
- Illumination correction using a "dark sky illumination" image.
- Remapping to a tangent plane projection with constant pixel size.
- Transient masking with multiple exposures.
- Single-band coadding of remapped exposures with significant overlap.

The CP is run by NOAO staff on all the community DECam data and the reduced images are generally available a week or so after the end of an observing run and available via the NOAO Science Archive[33]. The CP produces instrumentally calibrated images ("InstCal"), remapped versions of InstCal ("Resampled"), and single-band coadded images ("Stacked"). For SMASH we use the InstCal images which come in three multi-extension (one per chip) and fpack[34] compressed FITS files per exposure: flux ("image"), weight/variance ("wtmap"), and quality mask ("qmask").

4.2. *Pre-Processing with SMASHRED*

The CP-reduced images are not in a format that is readable by DAOPHOT. Therefore, we run a SMASH pre-processing script (`SMASHRED_PREP.PRO`) on the CP images for each night before PHOTRED is run. This script performs the following steps:

1. Rename files in the old ("tu") naming convention to the new ("c4d") convention.
2. Move standard star exposures to the "standards/" directory since they are processed separately from the science data.
3. Uncompress the FITS files, set "bad" pixels to 65,000, and write new FITS files for each chip.

[33] https://www.portal-nvo.noao.edu

[34] https://heasarc.gsfc.nasa.gov/fitsio/fpack/

4. Sort the exposures into PHOTRED "fields" based on the pointing and exposure times (short and long exposures are processed separately). Rename the files using the PHOTRED file naming convention (`FIELD#-EXPNUM#_CHIP#.fits`, e.g., `F5-00507880_17.fits`).

5. Download astrometric reference catalogs for each field and write separate reference catalog files for each chip FITS file.

6. Move files for each field into a separate directory (e.g., `F5/`).

The masks provide information on bad pixels, saturation, bleed trail, cosmic rays, and multi-exposure transients (or difference detections). There were some problems with the difference detections so we ignored that information in the mask. Any pixels that were affected by the other issues were set to a high value (65,000) so that PHOTRED/DAOPHOT would see these pixels as "bad".

4.3. *Nightly DECam PHOTRED Reduction*

Accurate, point-spread-function (PSF) fitting photometry was obtained using the automated PHOTRED pipeline first described in Nidever et al. (2011). PHOTRED performs WCS fitting, single-chip PSF photometry as well as multi-exposure forced-PSF photometry using the DAOPHOT suite of programs (Stetson 1987, 1994). PHOTRED was run separately on each night. The short and long exposures of a field were run through PHOTRED separately (the former with a "sh" suffix added to their name) and multi-band image stacking and forced photometry were only performed on the long exposures. This was mainly because of issues with bright, saturated stars when stacking short and long exposures and the fact that the short exposures did not add much to the overall depth of the longer exposures. Note also that deep exposures of a field taken on different nights were processed separately and only combined during the calibration stage (section 5).

PHOTRED is based on methods and scripts developed by graduate students and postdocs in S. Majewski's "halo" group at the University of Virginia (UVa) in the late 1990s and early 2000s (in particular J. Ostheimer, M. Siegel, C. Palma, T. Sohn & R. Beaton). PHOTRED was an attempt to fully automated these scripts (and some manual procedures) into a robust and easy-to-use pipeline. Most of the PHOTRED software was written by D.L.N. in 2008 while he was a graduate student at UVa and has been continually updated and improved since then. PHOTRED consists of IDL[35] driver programs wrapped around the DAOPHOT fortran routines, but also includes some IRAF, fortran and unix shell scripts.

PHOTRED currently has 13 "stages". Text-based lists are used for keeping track of inputs, outputs and failures and shuffling files from one stage to the next. This is overall design was taken partly from the SuperMACHO "photpipe" pipeline (Rest et al. 2005; Miknaitis et al. 2007). The global parameters and optional settings (see the github repository for the full list) as well as the stages to be run are specified in the `photred.setup` setup file. The stages are described more fully below.

4.3.1. *RENAME*

The headers are checked for all the required keywords (gain, read noise, time stamp, filter, exposure time, α/δ, airmass). The exposures are grouped into "fields" based on values in the "object" keyword in the header and renamed with the PHOTRED naming convention (`FIELD#-EXPNUM#_CHIP#.fits`). The PHOTRED short field names and full field names are saved in the `fields` file. This stage was skipped for SMASH since it is already performed by the `SMASHRED_PREP.PRO` pre-processing script.

4.3.2. *SPLIT*

If the FITS files are multi-extension files then these are split into separate FITS files per chip. This was stage was also skipped for SMASH.

4.3.3. *WCS*

The world coordinate system (WCS) for an image is created (or refined if it already exists in the header) by using an astrometric reference catalog and some information about the imager (pixel scale and orientation) and pointing (rough α/δ of the center of the image, normally from the telescope TCS system). The software (`WCSFIT.PRO`) performs its own simple source detection, sky estimation and aperture photometry of the image using routines from the IDL Astronomy User's Library[36]. If a WCS does not already exist, then the reference catalog α/δ values are transformed roughly to the X/Y cartesian coordinates of the image by using the exposure and image information provided. The reference sources are then cross-matched with the image sources by cross-correlating down-sampled "detection" map images of the two groups of sources. The peak in the cross-correlation image is used to obtain an initial measurement of the X/Y offsets between the lists and the significance of the match. If a significant match is found then nearest-neighbor matching is performed with a large matching radius and the measured offsets. The matches are used to fit a four parameter transformation matrix (essentially translation, rotation and scale) and second round of improved nearest-neighbor matching. The final matches are used to perform fitting of the four `CD#_#` and two `CRVAL#` parameters of the WCS. The software does not create or modify existing higher-order distortion terms.

By default, the SMASHRED pre-processing used USNO-B1[37] (Monet et al. 2003) as the astrometric reference catalog, and sometimes 2MASS or UCAC-4. After the first Gaia data release (Gaia Collaboration et al. 2016), the WCS-fitting software was rerun with Gaia as the astrometric reference and the resulting FITS header (with the improved WCS) saved in a separate text file (`gaiawcs.head`) for each image. The astrometric solutions were dramatically improved with RMS$\sim$20 mas (Figure 3).

[35] The Interactive Data Language is a product of Exelis Visual Information Solutions, Inc., a subsidiary of Harris Corporation.

[36] http://idlastro.gsfc.nasa.gov

[37] http://tdc-www.harvard.edu/catalogs/ub1.html

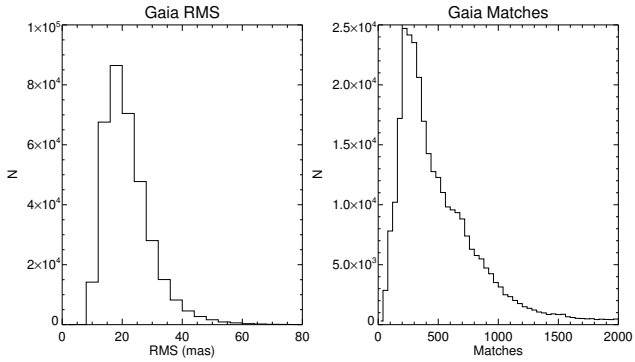

FIG. 3.— (Left) The distribution of RMS values between the Gaia astrometric reference catalog and the SMASH DECam data for the final WCS (for the ∼350,000 SMASH chips). (Right) The distribution of matches between the SMASH and Gaia data.

4.3.4. *DAOPHOT*

This stage detects sources in the single exposure images, constructs the PSF, and uses it to measure PSF photometry with ALLSTAR. There are several steps:

PSF FWHM Estimate: Since DAOPHOT requires an estimate of the PSF FWHM (or seeing) to work a custom IDL routine (`IMFWHM.PRO`) with independent algorithms is used to make this estimate. It detects peaks in the image 8σ above the background (although this is lowered if none are detected) and keeps those that are the maximum within 10 pixels and have two or more neighbors that are brighter than 50% of its flux. It then finds the contour at half-maximum flux in a 21×21 sky-subtracted sub-image centered on the peak and uses it to measure an estimate of the FWHM (2× the mean of the radius of the contour) and the ellipticity of the contour. In addition, the total flux in the subimage and the DAOPHOT "round" factor (using marginal sums) are computed. These metrics are then used to produce a cleaner list of sources (FWHM>0, round<1, ellipticity<1 and flux<0) on which two-dimensional Gaussian fitting is performed and more reliable metrics are computed. The final list of sources is selected by cuts on the new metrics and the distributions of semi-major, semi-minor axes and χ^2 (they must lie in the dominant clustering of sources). The final FWHM and ellipticity are then computed from these sources using robust averages with outlier rejection. This FWHM value is then used in the step next to set the DAOPHOT input options.

DAOPHOT option files: Both DAOPHOT and ALLSTAR require option files (`.opt` and `.als.opt` respectively). Some of the most important default settings are shown in Table 2.

For some very crowded fields (e.g., Field35 and Field46), the default settings produced suboptimal results and linear PSF spatial variations (`VA`=1) and a smaller fitting radius (`FI`=0.75×FWHM) were used. The affected nights are 20141123, 20141217, 20151205 and 20151206.

Common sources list: Early on in the development of PHOTRED there were issues with constructing good PSFs for the deep (280 second), intermediate-band DDO51 observations for the MAPS survey (Nidever et al. 2011, 2013, which was the main motivation for writing PHOTRED). This was because there were a lot of point-like cosmic rays that overwhelmed the small number of real sources and made it difficult to create a good PSF source list just by culling via morphology parameters. To deal with this problem, PSF sources were required to be detected in multiple images to make sure they were real objects. In this step, a "common sources list" is constructed for each file and later used as the starting point to select PSF stars. In the DECam data, the original issue is not as much of a problem because of the broad-band filters and cosmic rays tends to be more "worm"-like and less point-like. However, we have continued to use the common sources option in the DAOPHOT stage for SMASH.

TABLE 2
DEFAULT PHOTRED OPTIONS FOR DAOPHOT

Option	Comment
TH = 3.5σ	Detection threshold
VA = 2	Quadratic spatial PSF variations
FI = 1×FWHM	PSF fitting radius
AN = −6	Use lowest χ^2 analytical PSF model

Detection: Sources are detected in the images with `FIND`, and aperture photometry is determined with `PHOTOMETRY` with an exponential progression of apertures from 3 to 40 pixels and sky radius parameters of 45 (inner) and 50 (outer) pixels.

Construct PSF: The PSF is constructed with an iterative procedure for culling out of "suspect" sources. The initial list of 100 PSF sources is selected using `PICK` from the common source list (or the aperture photometry file if the common source option was not used) and a morphology cut is applied ($0.2 \leq$ sharp ≤ 1.0; using the sharp produced by `FIND`) to remove extended objects. The list is then iteratively cleaned of suspect sources. At each iteration a new PSF is constructed with `PSF` using the new list and DAOPHOT prints out the χ^2 (root-mean-square residual) for each star and flags any outliers (`?` and `*` for 2 and 3 times the average scatter, respectively). The flagged outliers and any sources with χ^2>0.5 are removed from the list and the procedure is started over again until no more sources are rejected.

After the list has converged, sources neighboring the PSF sources (using `GROUP`) are removed form the image (using `SUBSTAR`). A new PSF is constructed from this "neighbors subtracted" image and a similar iterative loop is used to remove PSF outlier sources.

Run ALLSTAR: ALLSTAR is run to perform simultaneous, PSF fitting on all the detected sources in the image using the constructed PSF. The default PHOTRED setting is to allow ALLSTAR to recentroid each source. ALLSTAR is also run on "neighbors subtracted" image to obtain PSF photometry for the PSF stars that is later used to calculate an aperture correction. ALLSTAR output X/Y centroids, magnitudes with errors, sky values, as well as chi and sharp morphology parameters (`.als` file).

One of the failure modes for a file in this stage is to not have enough PSF stars after the cleaning to constrain the solution. In these cases the PSF spatial variation value (`VA`) was lowered in the option file by hand and DAOPHOT was rerun. This solved the failures in the large majority of cases. For the small number of files

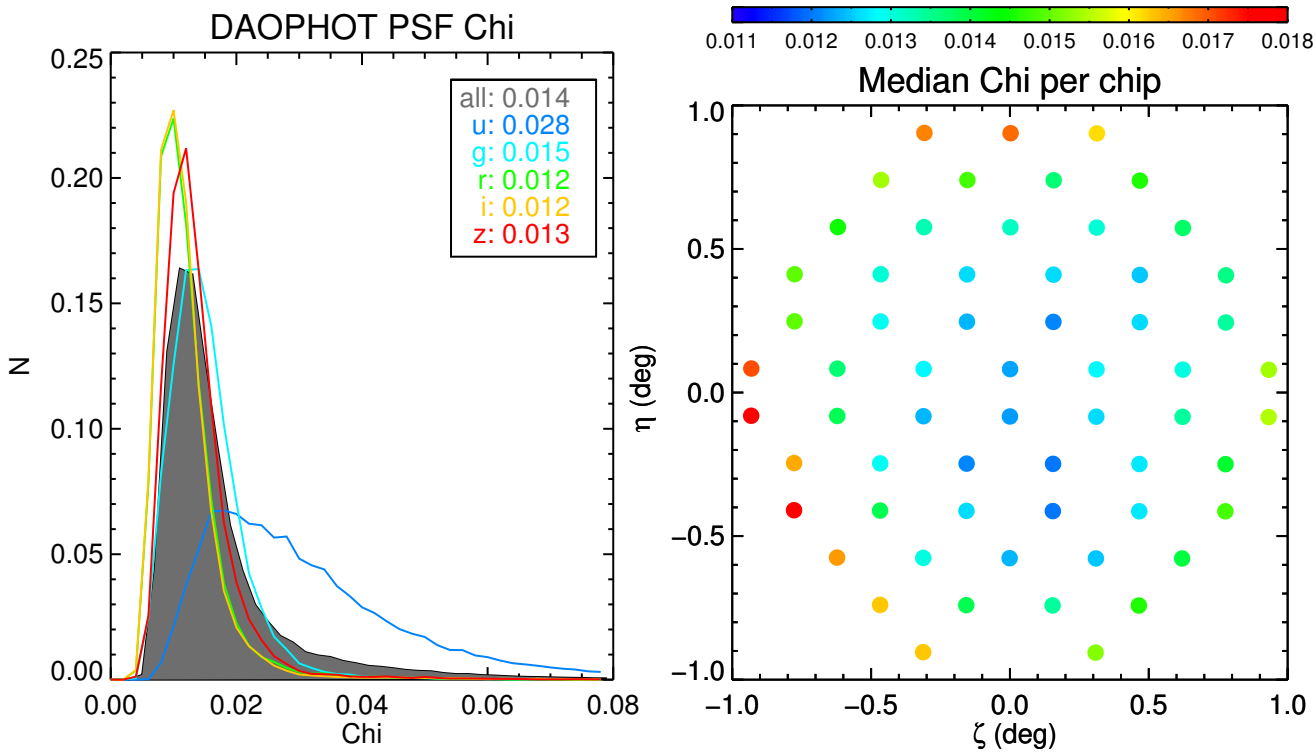

FIG. 4.— (Left) The distribution of DAOPHOT PSF "chi" values (relative root-mean-square of the analytic PSF residuals) for the ∼350,000 SMASH chips broken down by band. The median values per band are given in the legend. (Right) The median chi value per chip as they appear in the focal plane.

where this also failed, we selected PSF sources by visual inspection of the sources. The procedure will be modified in the future to start with a simple, constant analytic PSF and slowly add more complexity if it is needed which should avoid these problems.

Figure 4 shows the histogram of DAOPHOT analytic PSF "chi" values (root-mean-square of the analytic PSF residuals relative to the peak height) broken down by band. Note that any systematic differences between the true PSF and the analytic first approximation go into the DAOPHOT PSF look-up table of corrections, so the true RMS of the residuals are actually smaller. The *griz* chi values are tighly peaked around ∼0.012 (or 1.2%) while the *u*-band values are a factor of 2× larger. The right-hand panel shows the median chi value per chip as they appear on the sky, indicating that the analytic first approximations are slightly poorer for the chips on the periphery of the focal plane. Figure 5 shows diagnostic thumbnails of median-combined relative flux residuals from PSF-subtracted images of many bright stars. The PSF relative flux error is on the order of ∼0.3% with very little systematic structure left in the medianed residual image indicating that the PSFs are of high quality.

4.3.5. *MATCH*

The sources in the ALLSTAR photometry catalogs from the DAOPHOT stage are cross-matched and combined with the files for each chip being handled separately (i.e., all the chip 1 files are cross-matched together and the chip 2 file are cross-matched together, etc.). Astrometric transformations between the frames (using the X/Y cartesian coordinates) and a reference frame (which is chosen based on the longest exposure time frame in the `filtref` band) are computed (in similar manner to what DAOMATCH achieves). The WCS in the FITS headers are used to calculate an initial estimate of the transformations. If this fails, then a more general matching routine is run that uses a cross-correlation technique of a down-sampled "detection" map image between the two source lists (as described above in section 4.3.3). Once all the transformations are in hand, DAOMASTER is used to iteratively improve the transformations (written to `.mch` file) and cross-matches, and, finally, combine all of the photometry into one merged file (the `.raw` file).

4.3.6. *ALLFRAME*

The PSF photometry can be improved by using a stacked image for source detection and then holding the position of the sources fixed while extracting PSF photometry from each image. The improvement of this "forced" photometry over regular PSF photometry done separately from each image comes from the reduced number of parameters (i.e., the positions). PHOTRED makes use of the DAOPHOT ALLFRAME (Stetson 1994) program to perform the forced photometry.

This stage performs several separate tasks:

1. **Construct multi-band coadd:** A weighted average stack is created of all the images. First, the relative scaling, sky level, and weights are computed for all the images. The weights are essentially the S/N and based on sources detected in all of the images (if no sources are detected in all the images, then a bootstrap approach is used to tie the images to one another). Second, images are transformed to a common reference frame. The

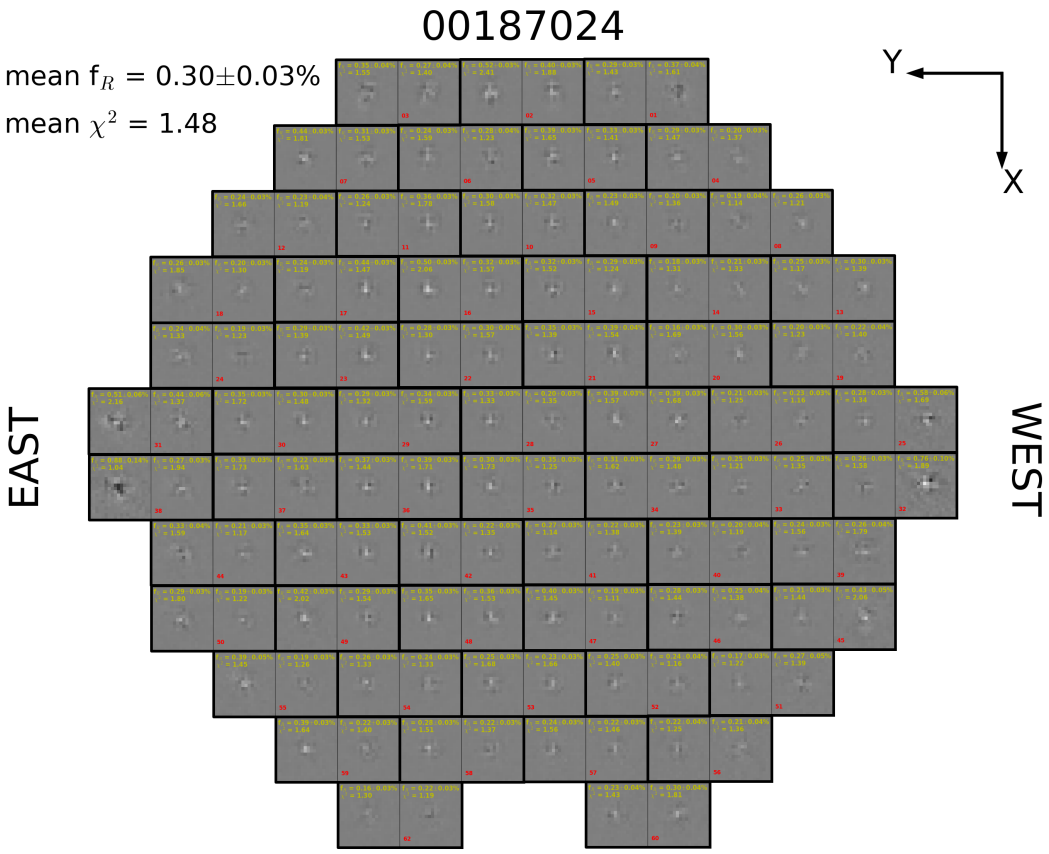

FIG. 5.— PSF quality assurance figure. Relative residuals in the PSF-subtracted image (relative to total flux in the PSF model) medianed across ∼30 high S/N stars per half-chip. Each horizontal rectangle represents one chip of an exposure, and the two squares one half of the chip. The relative absolute residuals and the uncertainties (using propagation of errors from the noise in each image) as well as the χ^2 for each half-chip are shown in the top of each square in yellow. The range of the greyscale is ±0.2% and the chip number (CCDNUM) is shown in red

original code only applied X/Y translations to the images. However, this was insufficient for larger dithers where the higher-order distortions become important and the software was rewritten to fully resample the images onto the final reference frame. The type of transformation used can be found in the `ALFTILETYPE` column ("ORIG" or "WCS") of the final `chips` catalog/table. Finally, the images are average combined using the IRAF routine IMCOMBINE with bad pixel masking and outlier rejection (sigma clipping). The gain in the header is maintained because the images are scaled to the reference exposure. However, new read noise and sky values[38] for the combined image (`_comb.fits`) are computing using the weights, scalings and sky values. It is challenging to preserve the fidelity of bright stars when combining deep and shallow exposures. This is one reason why it was decided to process short and long SMASH exposures separately in PHOTRED.

2. **PSF construction:** The PSF of the combined image is constructed using the same routine as in the DAOPHOT stage.

[38] Sky is needed in the combined images since DAOPHOT uses it as part of its internal noise model.

3. **Iterative source detection:** Source detection is performed iteratively in two steps. (1) Source detection with Source Extractor (SExtractor; Bertin & Arnouts 1996) on the working image (PSF subtracted after the first iteration). (2) ALLSTAR is run on the original image (with the PSF found in the previous step) using the current master source list and subtracts sources that have converged. The output from ALLSTAR from the last iteration is used as the final master source list (`_comb_allf.als`). The detection settings for SExtractor are: use a convolution filter, $>1\sigma$ detection threshold, and a minimum area of 2 pixels per source. Normally only two iterations are used since we found that after that any new detections are mainly noise.

4. **Run ALLFRAME:** ALLFRAME is run on all the images using their respective PSFs and the master source list constructed in the previous step. ALLFRAME uses the coordinate transformations between images from the `.mch` file (in the MATCH stage), but computes its own small, high-order geometric adjustments (we use 20 terms or cubic in X and Y) to these during the fitting process (it slowly adds in the higher orders to keep the solutions constrained). We allow a maximum of 50

iterations in ALLFRAME after which it outputs catalogs (`.alf`) with X/Y coordinates (in that image's reference frame), photometry with errors and chi and sharp morphology parameters.

After ALLFRAME has finished, the results for the individual images are combined and the SExtractor morphology parameters are added to the final catalog (`.mag` file).

It is possible to skip the ALLFRAME stage for certain fields by specifying them in the `alfexclude` option of the `photred.setup` file.

4.3.7. *APCOR*

The DAOPHOT program DAOGROW (Stetson 1990) is used to produce growth-curves for each band and night separately. These are used to produce "total" photometry (including the broad wings) for the bright PSF stars for each chip. These values are then compared to the PSF photometry values for these object (from neighbor subtracted images), produced in the DAOPHOT stage, to compute an average aperture correction for each chip. These are all stored in the `apcor.lst` file and used later in the CALIB stage.

4.3.8. *ASTROM*

The WCS in the FITS header is used to add the α and δ coordinates for each object to the catalog.

4.3.9. *CALIB*

The photometry is calibrated using the transformation equations given in the transformation file specified in `photred.setup` (e.g., `n1.trans`). The equations in the file can have various levels of specificity: (1) only the band is specified, (2) the band and chip are specified, or (3) the band, chip and night are specified. The terms in the transformation file are zero-point, extinction, color, extinction×color, and color^2 with their uncertainties. Besides these corrections the photometry is also corrected for the exposure time and the aperture correction (for that chip.

Since the *calibrated* color is meant to be used for the color term, the software uses an iterative method to calibrate the photometry (using an initial color of zero). A (weighted) average value is used for the other band to construct the color (if multiple exposures in that band were taken) but not for the band being calibrated (the value for that exposure is used). Also, a color of zero is used for objects for which a good color cannot be constructed. The loop continues until convergence (all magnitude differences are below the 0.0001 magnitude level or 50 iterations, whichever is first).

Calibrated photometry for each exposure (e.g., `G5`) are given in the output file and optionally the average magnitudes per band (e.g., `GMAG`) and the instrumental magnitudes for each exposure (e.g., `I_G5`). Since for SMASH a global calibration strategy was adopted, all of the values in the transformation file were set to zero so that the photometry was only corrected for the exposure time and aperture corrections.

4.3.10. *COMBINE*

The individual chip catalogs are combined to create one catalog for the entire field. Sources detected in multiple chips (from dithered exposures) are combined and their photometry combined. The default matchup radius is $0.5''$.

4.3.11. *DEREDDEN*

citetSFD98 E$(B-V)$ extinction values are added to the final, combined catalog for each source. Extinction (A$[X]$) and reddening (E$[X-Y]$) values for the bands and colors specified in the `photred.setup` setup file (using A$[X]$/E$[B-V]$ values from the given `extinction` file) are also added.

4.3.12. *SAVE*

The final ASCII catalog is renamed to the name of the field (e.g., `F5` is renamed to `Field62`) and a copy is created in the IDL "save" and FITS binary table formats. In addition, a useful summary file is produced with information on each exposure and chip for that field.

4.3.13. *HTML*

This stage creates static HTML pages to help with quality assurance of the PHOTRED results. Quality assurance metrics are computed and plots created for the pages. This stage was skipped for SMASH since custom quality assurance routines were written.

4.4. *Processing of Standard Star Data with STDRED*

The southern sky that SMASH is observing has not been well covered with *ugriz* CCD imaging, which means that it is not possible to calibrate our photometry with existing catalogs (in the same area of the sky) as can be done in the north with SDSS and Pan-STARRS1 (Kaiser et al. 2010) data. Therefore, we must use the traditional techniques of calibrating our data with observations of standard star fields (on photometric nights) and extra calibration exposures (for non-photometric nights). We use standard star data taken in the SDSS footprint along the celestial equator and downloaded "reference" catalogs via CasJobs[39] and DR12 (Alam et al. 2015).

To reduce the DECam standard star exposures we use the STDRED pipeline, which is a sister package to PHOTRED and works in a similar manner. The same t smashred_prep.pro pre-processing script is used to uncompress, mask and split the CP-reduced imaged and download the astrometric reference catalogs per field. The main STDRED steps that are used by SMASH are:

- WCS: Fits the chip WCS using the astrometric reference catalog.
- APERPHOT: Detects sources and measures aperture photometry.
- DAOGROW: Calculates aperture corrections via curves of growth and applies them to the aperture photometry.
- ASTROM: Adds α/δ coordinates to the photometric catalog.

[39] http://casjobs.sdss.org

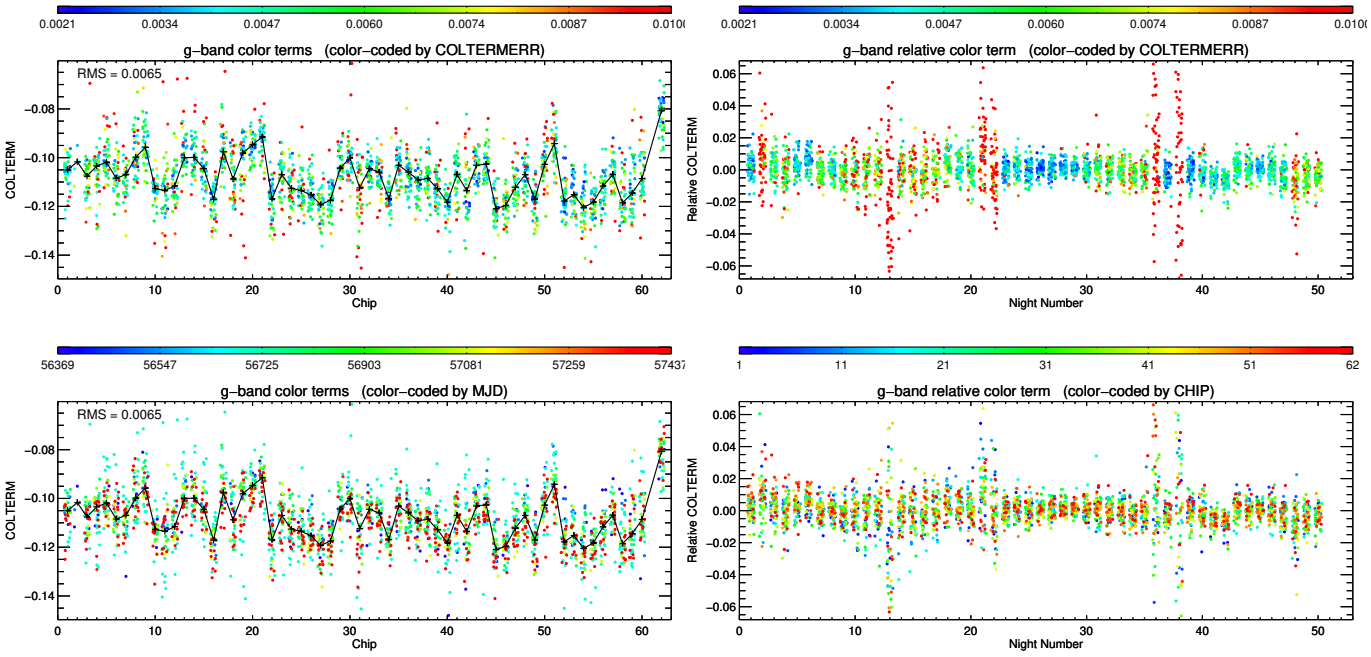

FIG. 6.— The color terms of the photometric transformation equations. (Left) Dependence on chip and (right) temporal dependence (night number is a running counter). REMOVE THE LOWER PANELS.

- MATCHCAT: Matches the observed catalog with the reference catalog and outputs information from both for the matches.
- COMBINECAT: Combine all of the matched photometry for a given filter.
- FITDATA: Fit photometric transformation equations (with zero-point, color, and extinction terms) for each filter using all of the data.

The standard star exposures from each DECam run are processed with STDRED in their own directory. The process of deriving the final SMASH DECam photometric transformation equations are described in Section 5.1.

4.5. *Reduction of the 0.9-m data*

4.5.1. *Image processing*

We used the NOAO/IRAF QUADRED package, custom IDL programs, and other software to process the images from the 0.9-m observations. The basic steps consisted of:

1. Electronic crosstalk correction, using custom software to measure and correct for the electronic ghosting present in the images when read through multiple amplifiers
2. Correction for electronic bias using the CCD's overscan region and bias frames
3. Trimming of the images to the illuminated area
4. Derivation of the exposure time-dependent illumination map caused by the opening and closing of the camera's iris shutter using dome flat observations designed for the purpose, and application of this shutter shading correction to the observed images
5. Derivation of flat field frames from twilight sky images and application to the object frames
6. Derivation of a bad pixel mask from dome flat observations designed for the purpose, with bad pixel correction applied to the object frames
7. Derivation of dark sky flats (*ugri*) and fringe frames (*z*) by stacking and filtering the deep sky observations taken throughout each observing run, followed by division by the dark sky flats (*ugri*) and subtraction of fringe features (*z*) for all object frames
8. Use of the code library from http://astrometry.net (Lang et al. 2010) to populate the object image headers with World Coordinate System (WCS) solutions

4.5.2. *Photometry*

We performed photometry on the 0.9-m observations of SDSS standards and SMASH target fields with a pipeline based on the DAOPHOT software suite (by K.O., separate from PHOTRED/STDRED). In short, we used DAOPHOT to measure aperture-based photometry of the standard star frames, with a smallest aperture of 6″diameter and a largest aperture of 15″diameter. We used DAOGROW to measure the growth curve based on the aperture measurements and to extrapolate the total magnitudes of the standard stars. These total magnitudes were used to derive the photometric transformation equations from the standard star observations. We also measured PSF photometry of the SMASH target fields and the standards using DAOPHOT and ALLSTAR. We derived PSFs from the images using as many as 200 point sources per image, using an iterative method to remove

TABLE 3
0.9-m Photometric Transformation Equations (SDSS filter set)

Band	$(ABCDE)_1$	$(ABCDE)_2$	$(ABCDE)_6$	$(ABCDE)_7$
14 – 23 Feb 2014				
u	1.001 ± 0.002	0.51 ± 0.02	-0.034 ± 0.004	4.59 ± 0.04
g	0.997 ± 0.001	0.19 ± 0.01	0.009 ± 0.011	2.66 ± 0.03
r	0.995 ± 0.001	0.11 ± 0.01	-0.022 ± 0.007	2.67 ± 0.02
i	0.995 ± 0.002	0.06 ± 0.01	-0.017 ± 0.014	3.13 ± 0.03
z	0.998 ± 0.001	0.07 ± 0.02	0.040 ± 0.011	3.95 ± 0.02
25 Sep – 2 Oct 2014, 26 Apr – 3 May 2015, and 27 – 29 Nov 2015				
u	1.0	0.49 ± 0.02	-0.034	4.17 ± 0.29
g	1.0	0.18 ± 0.01	0.005	2.51 ± 0.31
r	1.0	0.10 ± 0.01	-0.028	2.49 ± 0.21
i	1.0	0.06 ± 0.01	-0.026	2.91 ± 0.12
z	1.0	0.06 ± 0.01	0.022	3.72 ± 0.05

neighbors from the PSF stars and to improve the PSF estimation. We applied aperture corrections to the PSF photometry by comparing the PSF meaurements with the total magnitudes from DAOGROW and fitting for the residuals with second-order polynomial function in x and y. These aperture-corrected PSF magnitudes were used as the basis of our standard magnitudes for the SMASH fields, while for the standard fields served as a consistency check between the aperture and PSF-based procedures, as described further below.

4.5.3. *Derivation of 0.9-m transformation equations*

Using the total magnitudes from DAOGROW, we explored fits to equations of the form:
$u_{\rm obs} = A_1 u + A_2 X + A_3 x + A_4 y + A_5 t + A_6 (u-g) + A_7$
$g_{\rm obs} = B_1 g + B_2 X + B_3 x + B_4 y + B_5 t + B_6 (g-r) + B_7$
$r_{\rm obs} = C_1 r + C_2 X + C_3 x + C_4 y + C_5 t + C_6 (g-r) + C_7$
$i_{\rm obs} = D_1 i + D_2 X + D_3 x + D_4 y + D_5 t + D_6 (r-i) + D_7$
$z_{\rm obs} = E_1 z + E_2 X + E_3 x + E_4 y + E_5 t + E_6 (i-z) + E_7$
where $u_{\rm obs} g_{\rm obs} r_{\rm obs} i_{\rm obs} z_{\rm obs}$ are instrumental magnitudes, *ugriz* are standard SDSS magnitudes drawn from Smith et al. (2002) and from SDSS DR12 (Alam et al. 2015), X is the airmass, x and y are pixel positions on the detector, and t is time of observation during the night.

We fit this set of equations first to the data taken on the almost entirely photometric run from 14 – 23 Feb 2014. Table 3 shows the best-fit coefficients. While we fit the transformation equations independently on each of the ten nights, we show only the average coefficients and their standard deviations in the table, as values were in all cases consistent across the nights. From our fits, we found no evidence for strong pixel position-dependent or time-dependent terms. We did, however, find evidence for a small magnitude-dependent scale factor of ∼0.5%, which may point to a small non-linearity or charge transfer efficiency issue with the aging Tek2K CCD.

We next explored fits to the equations for the observing runs 25 Sep – 2 Oct 2014, 26 Apr – 3 May 2015, and 27 – 29 Nov 2015. These runs were complicated by variable weather conditions, work on the camera electronics that changed the gain setting of the CCD, and by a temporary change from the CTIO SDSS *griz* filter set to the PreCam *griz* filter set that more closely matches the filter set used by DECam. For these observations, we fit the SDSS and PreCam sets separately. For each filter set, we first used all of the nights observed with that set to measure the color term coefficients. To do this, we allowed the zero point for each frame to be fit independently, which removes all other variables from consideration other than the color term; this allowed us to use standards taken on non-photometric nights to constrain the color term. We then fixed the color term coefficients to these fitted values, and for the photometric nights fit for the remaining coefficients on a per night basis. For these fits, we found no evidence for pixel position-dependent, time-dependent terms, or, in contrast to the Feb 2014 observations, a magnitude-dependent scale term. Table 3 shows the fitted coefficients and Figure 7 shows the photometric residuals for the standard star fields.

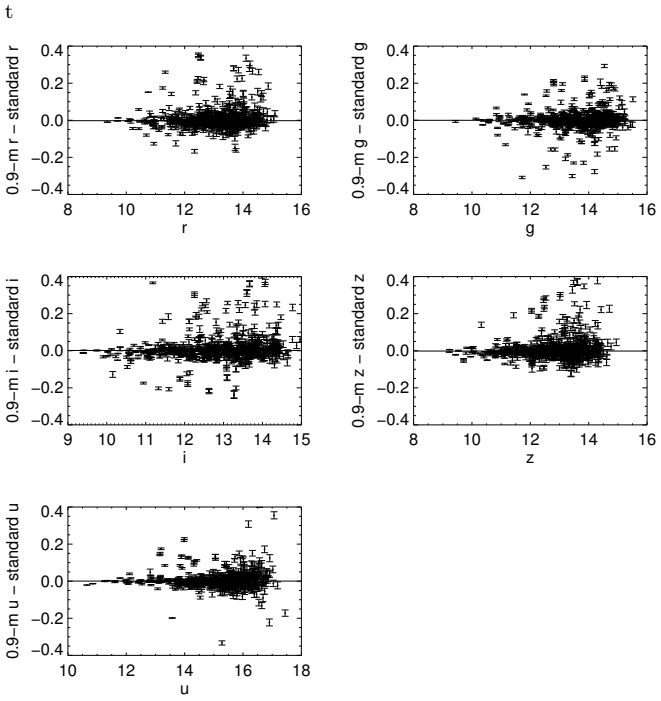

Fig. 7.— Residuals of the 0.9m photometry relative to the standard star data versus magnitude for the *ugriz* bands.

5. CALIBRATION

t

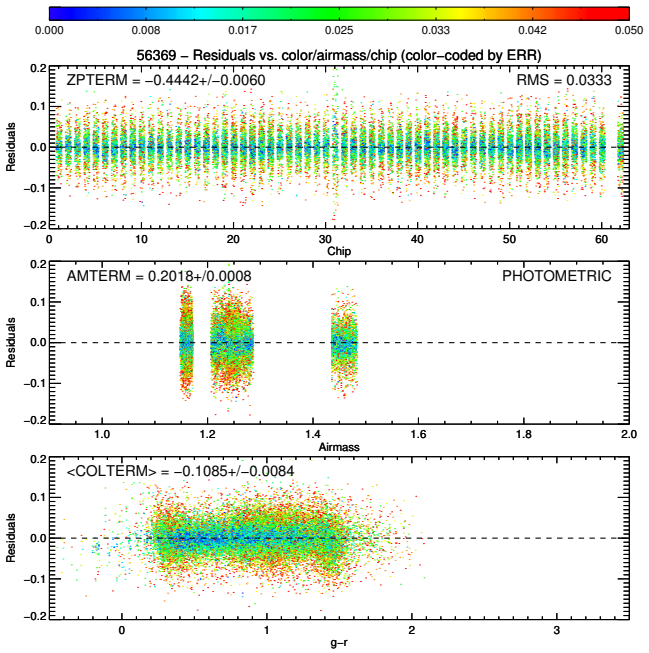

FIG. 8.— The residuals after fitting the photometric transformation equations to standard star observations for a typical photometric night (g-band). The observations are color-coded by their photometric error. (Top) Residuals versus chip number. (Middle) Residuals versus airmass. (Bottom) Residuals versus color.

5.1. *Derivation of Photometric Transformation Equations from Standard Star Data*

In order to produce the highest-quality and most uniform calibration we decided to write new custom software to determine the DECam photometric transformation equations using all of the standard star data together. The software (`solve_transphot.pro`) has several options for what variables to fit or hold fixed (zero-point, color, extinction, and color×extinction terms) and over what dimensions (e.g., night and chip) to average or "bin" values.

At first all variables (zero-point, color and extinction terms) were fit separately for each night and chip combinations to see how much the terms vary and over what dimensions.

Color: We found that the color terms vary from chip to chip (at the ∼0.01 mag level; Figure 6 left), but they appear to be temporally stable (Figure 6 right). Therefore, we fit the (linear) color terms for each chip separately by taking a robust average over all photometric nights.

No evidence for systematics was found in the color residuals of $g/i/z$ indicating there was no need for higher order color terms. For u-band there are systematics in the residuals (consistent across all fields) that would require higher order terms to fit. This is largely because of the different throughput curves for the SDSS and DECam filters. We decided not add higher order terms as these could adversely affect very blue or red objects (where the solution is not well constrained). However, to determine a uniform and reliable zero-point we decided to fit the shape in the residuals and remove this pattern from the observed data at the very beginning of the procedure. In addition, we restricted the color range to $1.0 < u\text{-}g < 2.5$. After this correction and color restriction are applied the residuals are flat. We similarly restrict the color range for r band ($g\text{-}r < 1.2$) because the correlation between SDSS and DECam r-band magnitudes becomes non-linear for redder stars due to the difference in the throughput curves.

Extinction: An appreciable number of nights had a small range in airmass for the standard star observations that produced unreliable extinction term measurements. Therefore, for these nights we calculated a weighted (by uncertainty and time difference) average of the extinction terms for the four closest neighboring good nights. Similarly, for nights with larger airmass ranges, we improve the accuracy to refitting the extinction term by using data from the four closest good neighboring nights (must be within 30 nights). Finally, we found that there was no appreciable color×extinction dependence and, therefore, these terms were not included in the fits.

Zero-point: We tried separating the zero-points into nightly zero-points and relative chip-to-chip (for each band but constant with time) zero-point offsets. The idea being that although the zero-point can change night-to-night, due to transparency and extinction variations, the zero-points of one chip to another (in a given band) should remain the same. We found, however, that the scatter in the relative chip-dependent zero-points over the many nights was higher than was anticipated and we obtained better results by fitting a zero-point for each night and chip combination. Therefore, we adopted the latter strategy and "abandoned" the relative zero-points (although they are computed and saved in the final output file).

Photometric nights are determined by seeing if the observer's noticed any sign of clouds, looking for cloud cover in the CTIO RASICAM all-sky infrared videos[40], and, finally, by looking at the scatter in the standard star residuals. The full list of nights for which STDRED was run and the photometric status are given in `smash_observing_conditions.txt` in `SMASHRED/obslog/`.

The ∼3100 variables were not fit to the data simultaneously but were found through an iterative fitting process:

1. Fit all terms separately for all night and chip combinations.
2. Compute the mean color term per chip.
3. Fix color terms and refit zero-point and extinction terms.
4. Average extinction terms. For nights with poor solutions or low airmass ranges a weighted average of the extinction terms of the nearest four neighboring nights is computed. For the rest of the nights, a new extinction term is computing using data included from the four nearest neighboring nights.
5. Fix color and extinction terms and refit zero-point terms.

[40] http://www.ctio.noao.edu/noao/node/2253

TABLE 4
SMASH Average Photometric Transformation Equations

Band	Color	Zero-point term	Color term	Extinction term
u	$u-g$	1.54326 ± 0.0069	0.0142 ± 0.0041	0.3985 ± 0.0024
g	$g-r$	−0.3348 ± 0.0019	−0.1085 ± 0.0010	0.1747 ± 0.00076
r	$g-r$	−0.4615 ± 0.0018	−0.0798 ± 0.0011	0.0850 ± 0.00098
i	$i-z$	−0.3471 ± 0.0016	−0.2967 ± 0.0012	0.0502 ± 0.00058
z	$i-z$	−0.0483 ± 0.0023	−0.0666 ± 0.0016	0.0641 ± 0.00075

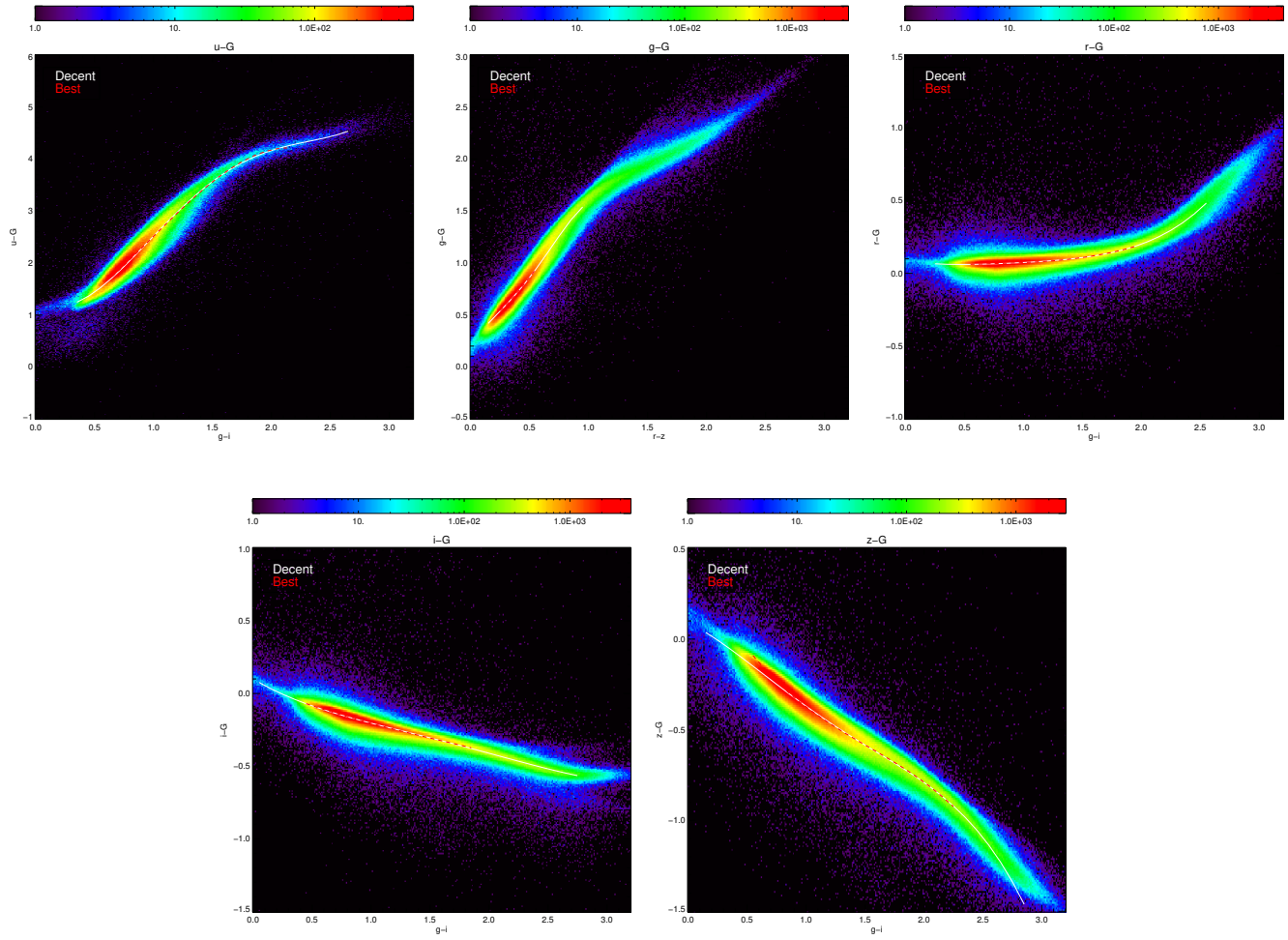

Fig. 9.— SMASH-Gaia color-color distributions and relations. While lines are polynomial fits over a "decent" color while the dashed red lines are polynomial fits over the color range giving the "best" and lowest scatter. The scatters over the best color ranges are u-6%, g-1%, r-0.2%, i-0.4%, z-0.5%.

The final photometric transformation equations are written to file (`smashred_transphot_eqns.fits` available in `SMASHRED/data/`) with zero-point, color and extinction terms (with uncertainties and averaging information) for each night and chip combination, as well as separate tables with information unique to each chip (e.g., color term) and information unique to each night (e.g., extinction term). The format uncertainties on the terms are: zero-point∼0.002, color∼0.0015, and extinction∼0.0007. For an average color and airmass this amounts to a formal uncertainty in the photometry of ∼0.002 mag (0.009 mag for u). Table 4 gives median values and uncertainties per band, while example residuals versus chip, airmass and color for a single night are shown in Figure 8.

The nights of the UT 2014 January 5–7 observing run were clear and photometric but no SDSS standard star observations were taken. Therefore, the regular procedures could not be used to determine the transformation equations for these nights. Subsequently some of the fields from this run could be calibrated because they were reobserved on other photometric nights (with standard star data) or 0.9m calibration data were obtained. The photometric transformation equations were then de-

termined ("backed-out") by using these calibrated fields and using the previously derived chip-dependent color terms. The `smashred_transphot_eqns.fits` was then updated with these values and the data for those nights could be calibrated in the regular manner.

5.2. *Calibration Software*

New software was developed to perform calibration of SMASH fields across multiple nights and using a variety of zero-point calibration methods. The software also takes advantage of the overlap of our multiple short exposures with large dithers to tie all of the chip data for a given field onto the same photometric zero-point using an ubercal technique.

The calibration follows these steps (in pseudocode):
WHILE until calibrated photometry changes <0.001 mag
• The photometry is calibrated using the zero-point (ZPTERM), color (COLTERM) and extinction/airmass terms (AMTERM). This is an iterative process because of the color-term. First, the source photometry is calibrated using the average photometry to construct the color (a color of zero is used on the first iteration), then the photometry is averaged per object and band. The process repeats until all changes are <0.0001 magnitude). (`SMASH_APPLY_PHOTTRANSEQN.PRO`)
FOR all filters
1) Measure the pair-wise photometric offsets of overlapping chips (`SMASH_MEASURE_MAGOFFSET.PRO`).
2) Solve the relative magnitude offsets per chip using the ubercal algorithm (`SMASH_SOLVE_UBERCAL.PRO`).
3) Determine the photometric zero-point (`SMASH_SET_ZEROPOINTS.PRO`).
ENDFOR
ENDWHILE

We employ a simple iterative ubercal solving technique. After all of the pair-wise photometric offsets of overlapping chips are measured, the robust weighted average offset of a chip relative to it's overlapping neighbors is calculated and one half of this is used as the ubercal correction for this chip. The pair-wise photometric offsets are updated for these chip-wise corrections and the procedure repeats until convergence is reached (the average relative offset change from one iteration to the next is less than 1%). The changes become very small after only a couple iterations. The cumulative corrections are applied to the chip-wise zero-point terms (`ZPTERM`) and saved in the `UBERCAL_MAGOFFSET` columns. The ubercal technique only measures and solves-for a constant magnitude offset for every chip. There is no allowance for spatial variations across the chip such as due to variable throughput (but see the QA section above). The outer (while) loop in the calibration is used to make sure the color terms are properly taken into account.

One of three different techniques is employed to set the photometric zero-point of the data depending on the observing conditions and what 0.9m calibration data are available. The options in decreasing order of preference are:

1. Photometric DECam data (`ZPCALIBFLAG`=1): Any DECam data taken during photometric conditions (`PHOTOMETRIC`=1) and having good photometric transformation equations from standard star exposures (`BADSOLN`=0) are used to set the photometric zero-point. Any non-photometric data are tied to this via the ubercal offsets.

2. Overlap with photometric DECam data (`ZPCALIBFLAG`=2): A field with no photometric data itself but that overlaps a neighboring field (this happens mainly in the central LMC and SMC fields) with photometric data can be calibrated using the overlap. The median offset of bright, high S/N overlap stars is used to set the zero-point.

3. 0.9m calibration data (`ZPCALIBFLAG`=3): If a field cannot be calibrated using the first two options and 0.9m calibration data are available for the field, then it is used to determine the zero-point with the stars detected in both the DECam and 0.9m data.

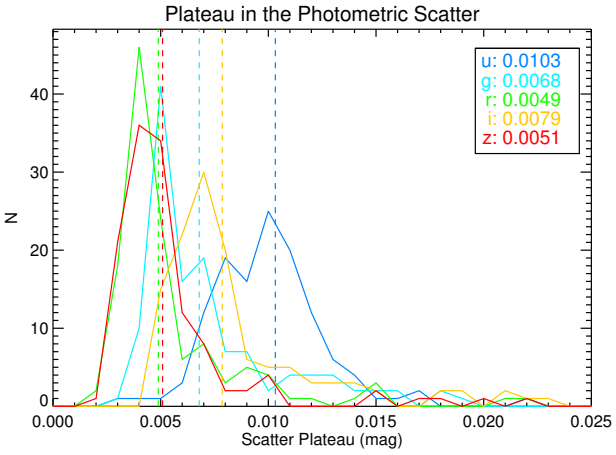

FIG. 10.— The distribution of the lower plateau in the photometric scatter (using multiple measurements of bright stars) in 126 calibrated SMASH fields. This a good estimate for the photometric precision of the survey. Vertical dashed lines show the median value for each band.

For fields where none of these options are available we use SMASH-Gaia color-color relations to calculate rough zero-points. These relations were derived by cross-matching with Gaia 49 SMASH fields with good, calibrated photometry and far from the LMC and SMC. Bright stars were used to determine the functional relationship between X_{SMASH}-G_{Gaia} and a SMASH color (g-i for all SMASH bands except r-z for g). These relations are very tight for the redder bands (r, i, and z) with only a scatter of ∼0.5% (see Figure 9), but are poorer and with large color term for the bluer bands (u and g with scatter of ∼6% and ∼1% respectively).

The photometric precision can be estimated by calculating the scatter in multiple independent measurements of the same object using bright stars. We measured the lower plateau in the photometric scatter for 126 deep and fully-calibrated SMASH fields in each band (Figure 10). The distributions indicate a precision of roughly 1.0% (u), 0.7% (g), 0.5% (r), 0.8% (i), and 0.5% (z) in the SMASH photometry. To evaluate the accuracy of the photometric calibration, we use the overlap of fields in the LMC/SMC main-body fields that are independently calibrated. Using the scatter in their distributions of

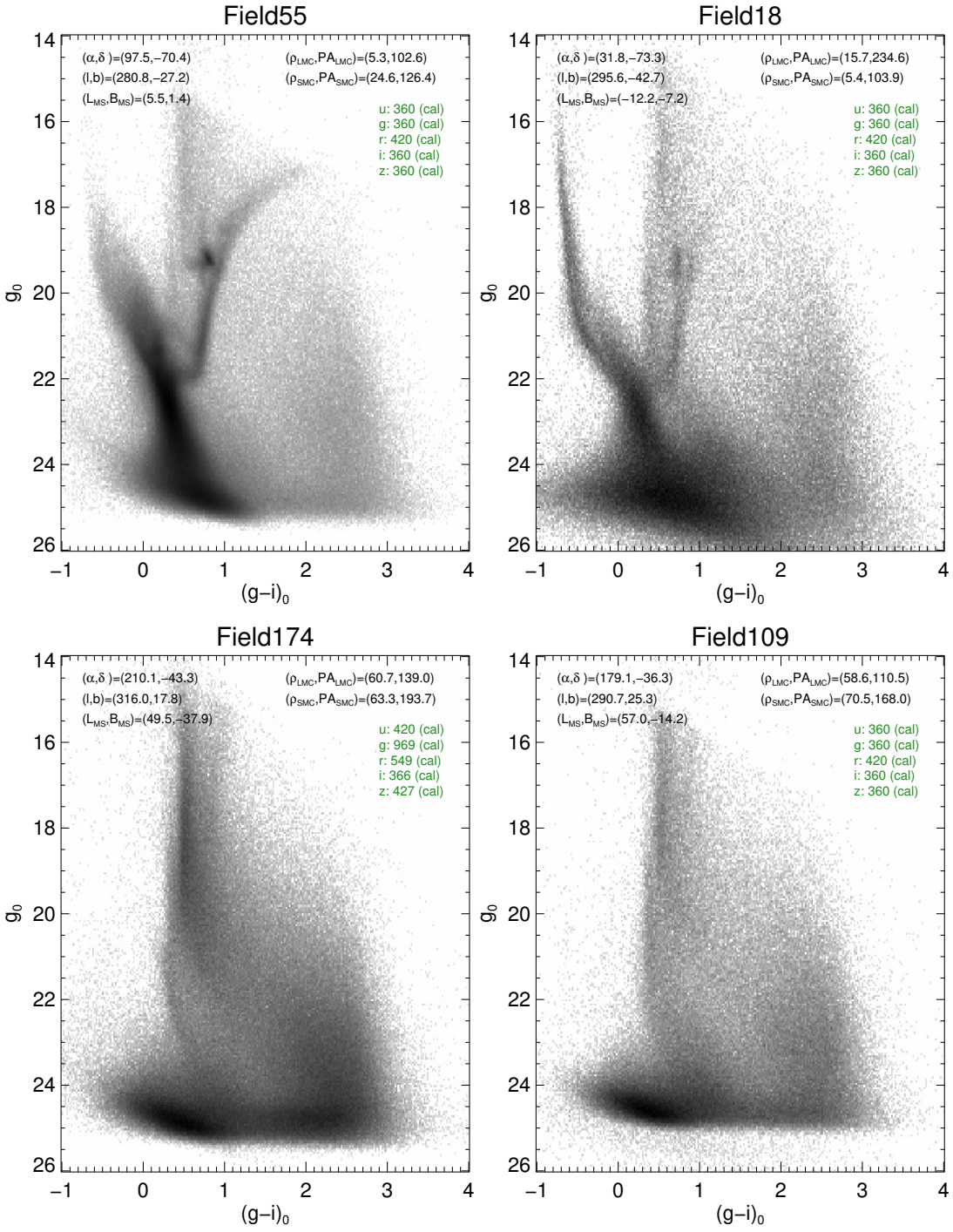

FIG. 11.— Some example SMASH Hess diagrams illustrating the depth and high-quality of the SMASH photometry and diversity of the stellar populations probed.

mean magnitude offsets (and accounting for the $\sqrt{(2)}$ because there are contributions from both fields) we obtain rough calibration accuracies of 1.3% (u), 1.3% (g), 1.0% (r), 1.2% (i), and 1.3% (z). The low scatter in the SMASH-Gaia color-color relations (especially for the redder bands) also attest to the high quality of the SMASH calibration.

Once all of the data are calibrated, average coordinates and morphological parameters (e.g., sharp, chi) are computed (weighted averages) from the multiple measurements of each object. We then product an exposure map for the field in each band (at the pixel level) and use this to sort out non-detections (set to 99.99) from cases of no good data for an object (set to NAN). Schlegel, Finkbeiner & Davis (1998) E(B-V) extinctions are also added for each object. Finally, the unique objects are cross-matched with the Gaia, 2MASS and ALLWISE catalogs.

The final catalogs consist of seven gzip-compressed binary FITS files per field:

1. `FIELD_exposures.fits.gz` – Information on each exposure.
2. `FIELD_chips.fits.gz` – Information on each chip.
3. `FIELD_allsrc.fits.gz` – All of the individual source measurements for this field.
4. `FIELD_allobj.fits.gz` – Average values for each unique object.
5. `FIELD_allobj_bright.fits.gz` – Bright stars from allobj used for cross-matching between fields.
6. `FIELD_allobj_xmatch.fits.gz` – Crossmatches between SMASH and Gaia, 2MASS and ALLWISE.
7. `FIELD_expmap.fits.gz` – The "exposure" map per band.

More detailed descriptions of the catalogs can be found in the PHOTRED "README" file[41] on the ftp site (see below).

The SMASH data processed to date includes 5,809 DECam exposures with 349,046 separate chip files producing 3,992,314,414 independent source measurements of 418,642,941 unique objects.

6. DESCRIPTION OF DATA RELEASE PRODUCTS

The first SMASH public data release contains ∼700 million measurements of ∼100 million objects in 61 deep and fully-calibrated fields sampling the ∼2400 deg^2 region of the SMASH survey (blue hexagons in Figure 2). The main data access is through a prototype version of the NOAO Data Lab[42]. Access and exploration tools include a custom Data Discovery tool, database access to the catalog (via direct query of TAP service), an image cutout service, and a Jupyter notebook server with example notebooks for exploratory analysis. The data release page also gives extensive documentation on the SMASH survey, the observing strategy, data reduction and calibration, as well as information on the individual data products.

Images, intermediate data products, and final catalogs (in FITS binary formats) are also available through the NOAO High Level Data Products FTP site[43]. The raw images as well as the CP-reduced InstCal, Resampled and single-band Stacked images are available in `raw/`, `instcal/`, `resampled/`, and `stacked/` directories, respectively (and grouped in nightly subdirectories). Each subdirectory has a `README` file that gives information about each FITS image file (e.g., exposure number, time stamp, filter, exposure time, field). The PHOTRED-ready FITS files and other associated files (PSF, photometry catalogs, logs, etc.) as well as the multi-band stacks are available in the `photred/` directory. The final binary FITS catalogs (as described in the last section) are in the `catalogs/` directory. Finally, there are seven tables in the database that were populated (slightly-modified) using the FITS catalogs: field, exposure, chip, source, object, and xmatch. The "field" table includes summary information for each field.

7. RESULTS

Figure 11 shows some example Hess diagrams of a number of our SMASH fields which indicate the depth (∼2 mag below the oldest main-sequence turnoff in the LMC) and high quality of the SMASH photometry.

The SMASH data have already produced some exciting results. In Martin et al. (2015), we presented the discovery of a compact and faint Milky Way satellite, Hydra II (in Field169), with morphological and stellar population properties consistent with being a dwarf galaxy (also see Kirby et al. 2015). Interestingly, comparison with simulations suggests that at Hydra II's position in the sky and distance of 134 kpc (from blue horizontal branch stars) it could be associated with the Leading Arm of the Magellanic Stream, although proper motion information is needed to confirm. We obtained follow-up time-series data on Hydra II to study its variable stars. This work yielded one RR Lyrae star in Hydra II that gave a slightly larger distance of 151 kpc as well as the discovery of dozens of short period variables in the field (Vivas et al. 2016).

Further sensitive searching for overdensities in the SMASH data yielded the discovery of a compact and very faint ($M_V = -1.0$) stellar system (SMASH 1) ∼11° away from the LMC. SMASH 1 is consistent with being an old globular cluster in the LMC periphery likely associated with the LMC disk and potentially on the verge of tidally disrupting.

One of the on-going SMASH projects is to map out the extended stellar populations of the LMC. An analysis of the Hess diagrams indicates that LMC stellar populations can be detected in SMASH data out to 21.1° from the LMC center, or ∼18.4 kpc, and to surface brightness levels of ∼33.3 mag/arcsec^2 (D. Nidever et al. 2017, in preparation).

One of the main goals of SMASH is to use the data in the central LMC/SMC fields to derive spatially-resolved star formation histories. The Hess diagram of Field55 in Figure 11 (upper left) is an example of the wealth of information in the data. This field, and other nearby ones, in particular, show two subgiant branches which indicates two periods of peak star formation. This was previously only seen in star formation rate diagrams from detailed star formation history modeling (Meschin et al. 2014), but now is visually clear just in the Hess diagrams. Full star formation history modeling still await computationally intensive artificial star tests for the SMASH data, which will be a focus of on-going SMASH processing efforts in the near future.

The deep and multi-band data in the main bodies of the Magellanic Clouds are also very useful for detecting faint star clusters. We are in the process of developing a citizen science project (led by L.C.J.) based on the SMASH data under the Zooniverse platform[44] which currently has roughly one million users and hosts many citizen science projects in multiple scientific disciplines. The project will be called "The Magellanic Project" and will be similar to the "The Andromeda Project" of *HST* images of M31. The citizen scientists will inspect our deep co-add ugriz images and visually identify (a) star clusters (open and globular), (b) galaxies behind the LMC/SMC

[41] ftp://archive.noao.edu/public/hlsp/smash/dr1/photred/README
[42] http://datalab.noao.edu/
[43] ftp://archive.noao.edu/public/hlsp/smash/dr1/
[44] https://www.zooniverse.org

main bodies, (c) and new dwarf galaxies of MW or the MCs. The website is projected to be launched in early 2017.

The SMASH data are also very useful for studying structures in the Milky Way halo that are unrelated to the Magellanic Clouds. The lower left panel of Figure 11 shows one field, not far above the Milky Way midplane, with a prominent stellar population at a distance of ∼10–20 kpc. Many other fields at low Galactic latitude show similar stellar populations that are very likely associated with the Monoceros "ring" (e.g., Slater et al. 2014). There are on-going SMASH projects to study these and similar MW halo structures in the SMASH data.

DLN was supported by a McLaughlin Fellowship while at the University of Michigan. EFB acknowledges support from NSF grant AST 1008342. M-RC acknowledges support by the German Academic Exchange Service (DAAD). TdB acknowledges financial support from the ERC under Grant Agreement n. 308024. SJ is supported by the Netherlands Organization for Scientific Research (NWO) Veni grant 639.041.131. DM-D acknowledge support by Sonderforschungsbereich (SFB) 881 "The Milky Way System" of the German Research Foundation (DFB). RRM acknowledges partial support from CONICYT Anillo project ACT-1122 and project BASAL PFB-06. GSS is supported by grants from NASA.

Based on observations at Cerro Tololo Inter-American Observatory, National Optical Astronomy Observatory (NOAO Prop. ID: 2013A-0411 and 2013B-0440; PI: Nidever), which is operated by the Association of Universities for Research in Astronomy (AURA) under a cooperative agreement with the National Science Foundation. This project used data obtained with the Dark Energy Camera (DECam), which was constructed by the Dark Energy Survey (DES) collaborating institutions: Argonne National Lab, University of California Santa Cruz, University of Cambridge, Centro de Investigaciones Energeticas, Medioambientales y Tecnologicas-Madrid, University of Chicago, University College London, DES-Brazil consortium, University of Edinburgh, ETH-Zurich, University of Illinois at Urbana-Champaign, Institut de Ciencies de l'Espai, Institut de Fisica d'Altes Energies, Lawrence Berkeley National Lab, Ludwig-Maximilians Universität, University of Michigan, National Optical Astronomy Observatory, University of Nottingham, Ohio State University, University of Pennsylvania, University of Portsmouth, SLAC National Lab, Stanford University, University of Sussex, and Texas A&M University. Funding for DES, including DECam, has been provided by the U.S. Department of Energy, National Science Foundation, Ministry of Education and Science (Spain), Science and Technology Facilities Council (UK), Higher Education Funding Council (England), National Center for Supercomputing Applications, Kavli Institute for Cosmological Physics, Financiadora de Estudos e Projetos, Fundação Carlos Chagas Filho de Amparo a Pesquisa, Conselho Nacional de Desenvolvimento Cientfico e Tecnológico and the Ministério da Ciência e Tecnologia (Brazil), the German Research Foundation-sponsored cluster of excellence "Origin and Structure of the Universe" and the DES collaborating institutions.

REFERENCES

Alam, S., Albareti, F. D., Allende Prieto, C., et al. 2015, ApJS, 219, 12

Bechtol, K., Drlica-Wagner, A., Balbinot, E., Pieres, A., Simon, J. D., Yanny, B., Santiago, B., Wechsler, R. H., Frieman, J., Walker, A. R., Williams, P., Rozo, E., Rykoff, E. S., Queiroz, A., Luque, E., Benoit-Levy, A., Bernstein, R. A., Tucker, D., Sevilla, I., Gruendl, R. A., da Costa, L. N., Fausti Neto, A., Maia, M. A. G., Abbott, T., Allam, S., Armstrong, R., Bauer, A. H., Bernstein, G. M., Bertin, E., Brooks, D., Buckley-Geer, E., Burke, D. L., Carnero Rosell, A., Castander, F. J., D'Andrea, C. B., DePoy, D. L., Desai, S., Diehl, H. T., Eifler, T. F., Estrada, J., Evrard, A. E., Fernandez, E., Finley, D. A., Flaugher, B., Gaztanaga, E., Gerdes, D., Girardi, L., Gladders, M., Gruen, D., Gutierrez, G., Hao, J., Honscheid, K., Jain, B., James, D., Kent, S., Kron, R., Kuehn, K., Kuropatkin, N., Lahav, O., Li, T. S., Lin, H., Makler, M., March, M., Marshall, J., Martini, P., Merritt, K. W., Miller, C., Miquel, R., Mohr, J., Neilsen, E., Nichol, R., Nord, B., Ogando, R., Peoples, J., Petravick, D., Plazas, A. A., Romer, A. K., Roodman, A., Sako, M., Sanchez, E., Scarpine, V., Schubnell, M., Smith, R. C., Soares-Santos, M., Sobreira, F., Suchyta, E., Swanson, M. E. C., Tarle, G., Thaler, J., Thomas, D., Wester, W., & Zuntz, J. 2015, ArXiv e-prints, arXiv:1503.02584

Belokurov, V., Irwin, M. J., Koposov, S. E., Evans, N. W., Gonzalez-Solares, E., Metcalfe, N., & Shanks, T. 2014, MNRAS, 441, 2124

Bertin, E., & Arnouts, S. 1996, A&AS, 117, 393

Besla, G., Kallivayalil, N., Hernquist, L., Robertson, B., Cox, T. J., van der Marel, R. P., & Alcock, C. 2007, ApJ, 668, 949

Besla, G., Kallivayalil, N., Hernquist, L., van der Marel, R. P., Cox, T. J., & Kereš, D. 2010, ApJ, 721, L97

—. 2012, MNRAS, 421, 2109

Besla, G., Hernquist, L., & Loeb, A. 2013, MNRAS, 428, 2342

Besla, G., Martínez-Delgado, D., van der Marel, R. P., et al. 2016, ApJ, 825, 20

The Dark Energy Survey Collaboration 2005, arXiv:astro-ph/0510346

, Drlica-Wagner, A., Bechtol, K., Rykoff, E. S., et al. 2015, ApJ, 813, 109

Gaia Collaboration, Brown, A. G. A., Vallenari, A., et al. 2016, A&A, 595, A2

Chabrier, G. 2001, ApJ, 554, 1274

Cioni, M.-R. L. 2009, A&A, 506, 1137

Deason, A. J., Belokurov, V., & Evans, N. W. 2011, MNRAS, 416, 2903

Deason, A. J., Belokurov, V., & Weisz, D. R. 2015, MNRAS, 448, L77

Deason, A. J., Wetzel, A. R., Garrison-Kimmel, S., & Belokurov, V. 2015, MNRAS, 453, 3568

D'Onghia, E., & Lake, G. 2008, ApJ, 686, L61

Diaz, J. D., & Bekki, K. 2012, ApJ, 750, 36 (DB12)

Gallart, C., Stetson, P. B., Meschin, I. P., Pont, F., & Hardy, E. 2008, ApJ, 682, L89

Gardiner, L. T. & Noguchi, M. 1996, MNRAS, 278, 191

Kallivayalil, N., van der Marel, R. P., Alcock, C., Axelrod, T., Cook, K. H., Drake, A. J., & Geha, M. 2006, ApJ, 638, 772

Kallivayalil, N., van der Marel, R. P., & Alcock, C. 2006, ApJ, 652, 1213

Kallivayalil, N., van der Marel, R. P., Besla, G., Anderson, J., & Alcock, C. 2013, ApJ, 764, 161

Jethwa, P., Erkal, D., & Belokurov, V. 2016, MNRAS, 461, 2212

Kaiser, N., Burgett, W., Chambers, K., et al. 2010, Proc. SPIE, 7733, 77330E

Koposov, S. E., Belokurov, V., Torrealba, G., & Wyn Evans, N. 2015, ArXiv e-prints, arXiv:1503.02079

Kirby, E. N., Simon, J. D., & Cohen, J. G. 2015, ApJ, 810, 56

Lynden-Bell, D. 1976, MNRAS, 174, 695

Mackey, A. D., Koposov, S. E., Erkal, D., et al. 2016, MNRAS, 459, 239
Majewski, S. R., Nidever, D. L., Muñoz, R. R., et al. 2009, IAU Symposium, 256, 51
Martin, N. F., Nidever, D. L., Besla, G., et al. 2015, ApJ, 804, L5
McConnachie, A. W. 2012, AJ, 144, 4
Meschin, I., Gallart, C., Aparicio, A., Hidalgo, S. L., Monelli, M., Stetson, P. B., & Carrera, R. 2014, MNRAS, 438, 1067
Monet, D. G., Levine, S. E., Canzian, B., et al. 2003, AJ, 125, 984
Miknaitis, G., et al. 2007, ApJ, 666, 674
Muñoz, R. R., Carlin, J. L., Frinchaboy, P. M., Nidever, D. L., Majewski, S. R., & Patterson, R. J. 2006, ApJ, 650, L51
Nidever, D. L., Majewski, S. R., & Burton, W. B. 2008, ApJ, 679, 432
Nidever, D. L., Majewski, S. R., Butler Burton, W., & Nigra, L. 2010, ApJ, 723, 1618
Nidever, D. L., Majewski, S. R., Muñoz, R. R., Beaton, R. L., Patterson, R. J., & Kunkel, W. E. 2011, ApJ, 733, L10
Nidever, D. L., Monachesi, A., Bell, E. F., Majewski, S. R., Muñoz, R. R., & Beaton, R. L. 2013, ApJ, 779, 145
Noël, N. E. D., Conn, B. C., Carrera, R., Read, J. I., Rix, H.-W., & Dolphin, A. 2013, ApJ, 768, 109
Olsen, K. A. G., Zaritsky, D., Blum, R. D., Boyer, M. L., & Gordon, K. D. 2011, ApJ, 737, 29
Rest, A., et al. 2005, ApJ, 634, 1103
Sales, L. V., Navarro, J. F., Cooper, A. P., White, S. D. M., Frenk, C. S., & Helmi, A. 2011, MNRAS, 418, 648
Schlegel, D. J., Finkbeiner, D. P., & Davis, M. 1998, ApJ, 500, 525
Skrutskie, M. F., Cutri, R. M., Stiening, R., et al. 2006, AJ, 131, 1163
Slater, C., Bell, E. F.,, Schlafly, E. F., et al. 2014, ApJ, 791, 9
Smith, J. A., Tucker, D. L., Kent, S., et al. 2002, AJ, 123, 2121
Stetson, P. B. 1987, PASP, 99, 191
Stetson, P. B. 1990, PASP, 102, 932
—. 1994, PASP, 106, 250
Valdes, F., Gruendl, R., & DES Project 2014, Astronomical Data Analysis Software and Systems XXIII, 485, 379
van der Marel, R. P., & Kallivayalil, N. 2014, ApJ, 781, 121
Vivas, A. K., Olsen, K., Blum, R., et al. 2016, AJ, 151, 118
Walker, M. G., Mateo, M., Olszewski, E. W., et al. 2016, ApJ, 819, 53
Wetzel, A. R., Deason, A. J., & Garrison-Kimmel, S. 2015, ArXiv e-prints, arXiv:1501.01972
York, D. G., Adelman, J., Anderson, J. E., Jr., et al. 2000, AJ, 120, 1579